

Article

Elastic Critical Moment for the Lateral–Torsional Buckling (LTB) Analysis of Structural Glass Beams with Discrete Mechanical Lateral Restraints

Dario Santo, Silvana Mattei and Chiara Bedon*

Department of Engineering and Architecture, University of Trieste, 34127 Trieste, Italy; dario.santo.ds@gmail.com (D.S.); silvana.mattei@phd.units.it (S.M.)

* Correspondence: chiara.bedon@dia.units.it (C.B.); Tel.: +39-040-558-3837

Received: 30 April 2020; Accepted: 27 May 2020; Published: 29 May 2020

Abstract: Structural glass beams and fins are largely used in buildings, in the form of primary load-bearing members and bracing systems for roof or facade panels. Several loading and boundary conditions can be efficiently solved by means of bonded composites that involve the use of laminated glass sections. Additionally, the so-obtained glass members are often characterized by high slenderness. To this aim, several literature studies were dedicated to the lateral–torsional buckling (LTB) behavior of laterally unrestrained (LU) glass elements, with the support of full-scale experiments, analytical models, or finite element (FE) numerical investigations. Standardized design recommendations for LU glass members in LTB are available for designers. However, several design issues still require “ad hoc” (and often expensive) calculation studies. In most of the cases, for example, the mechanical interaction between the structural components to verify involves various typologies of joints, including continuous sealant connections, mechanical point fixings, or hybrid solutions. As a result, an accurate estimation of the theoretical LTB critical moment for such a kind of laterally restrained (LR) element represents a first key issue toward the definition and calibration of generalized design recommendations. Careful consideration should be spent for the description of the intrinsic features of materials in use, as well as for a combination of geometrical and mechanical aspects (i.e., geometry, number, position of restraints, etc.). In this paper, the attention is focused on the calculation of the elastic critical buckling moment of LR glass beams in LTB. Existing analytical approaches of the literature (mostly developed for steel constructional members) are briefly recalled. An additional advantage for extended parametric calculations is then taken from finite element (FE) numerical analyses, which are performed via the LTBeam or the ABAQUS software codes. The actual role and the effect of discrete mechanical restraints are, thus, explored for selected configurations of practical interest. Finally, the reliability of simplified calculation approaches is assessed.

Keywords: structural glass beams; laminated glass sections; lateral–torsional buckling (LTB); discrete mechanical lateral restraints; analytical methods; finite element (FE) numerical modeling; design

1. Introduction and State of the Art

Structural glass is largely used in building, in the form of load-bearing components [1]. While harmonized European standards for structural designs are still in preparation [2–4], the last few years showed a huge spread of technical guidelines, codes of practice, and documents in support of designers [5–7].

For structural applications, glass members are typically characterized by a laminated resisting cross-section, in which viscoelastic bonding interlayers are required to offer a certain mechanical

coupling to the involved glass components (Figure 1a). Accordingly, for a given geometry, the load-bearing response of glass layers can vary significantly (Figure 1b). Among the available interlayers [8], it is in fact generally recognized that that the mechanical response of a general laminated section is strictly related to the actual properties and bonding efficiency of these films [9,10]. As a result, refined methods of analysis and characterization should be generally taken into account, in the elastic stage [10–12] or in presence of possible degradation effects [13–15].

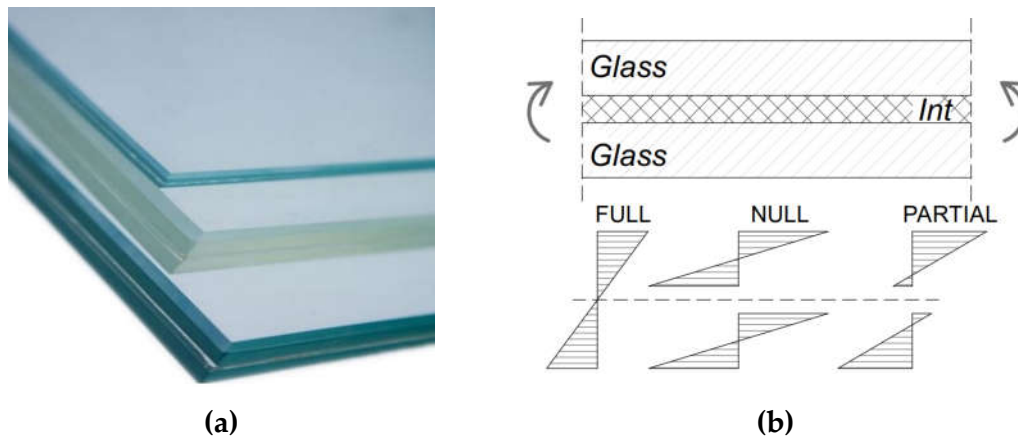


Figure 1. Laminated glass element: (a) cross-section examples and (b) corresponding stress distributions, depending on the shear coupling efficiency of the interlayers.

As far as glass beam-like elements are used to support and brace orthogonal facades or roofs, careful consideration in design should be spent to prevent premature lateral–torsional buckling (LTB) phenomena. Several research studies, in this regard, were dedicated to monolithic or laminated glass beams. Extended experimental investigations were reported in [16–21] for various LTB configurations of practical interest. The use of simplified, equivalent thickness-based formulations for laminated glass sections in LTB was explored in [22], toward the definition of reliable and standardized design buckling verification approaches [23–26]. These documents and most of the literature efforts, however, are generally focused on laterally unrestrained (LU) glass beams that roughly represent the actual load-bearing configuration of real fins (i.e., Figure 2).

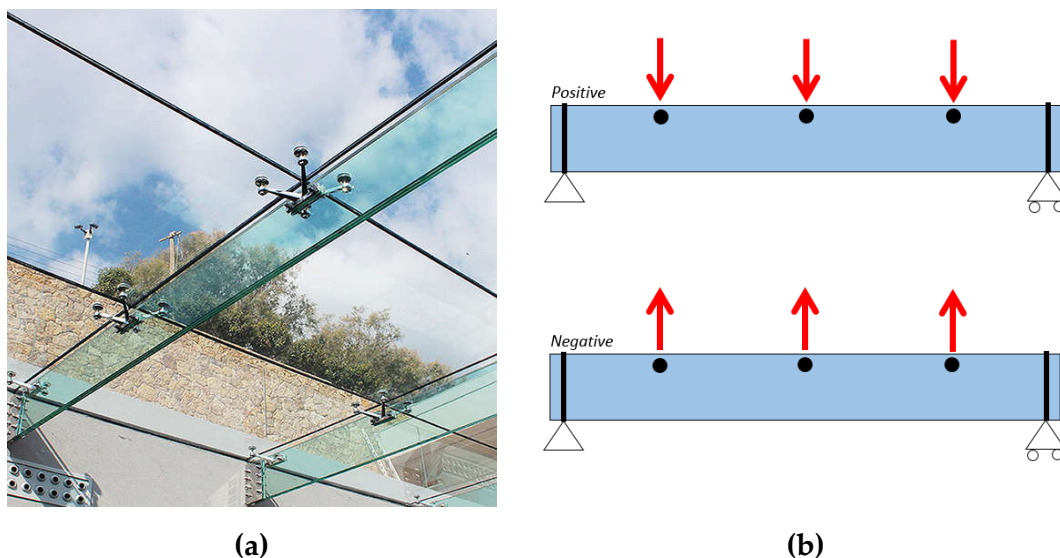


Figure 2. Example of (a) laterally restrained (LR) glass beams with discrete mechanical restraints and (b) typical loading configurations associated with positive or negative bending effects.

A limited number of background documents is currently available for laterally restrained (LR) glass members in LTB that can take advantage of the presence of possible bracing contributions, toward premature failure mechanisms. According to Figure 2a, for example, mechanical restraints can be used for fork-end supported, laminated glass fins acting as a bracing system for the interconnected orthogonal panels. The typical design loading conditions to assess are schematized in Figure 2b, where most of the imposed actions are expected to result in positive bending effects for the beams, while potential negative bending effects (i.e., due to suction wind) should also be taken into account. As long as the geometrical and mechanical features of the glass members and restraints in use are properly assessed, the LTB performance of LR systems according to Figure 2 is rationally expected to differ from a LU member with similar features. The LR features, moreover, can have substantially different efficiency, depending on the geometry of the members to verify.

Studies of the literature were reported in [27–29] for LR glass beams with continuous adhesive joints, giving evidence of the expected effects (and related calculation approaches) due to the presence of linear connections. In [29], the attention of finite element (FE) numerical analyses focused on LR glass beams with an adhesively restrained top edge, considering downward (i.e., positive bending moment effects) or upward (negative) design loads, as well as related LTB phenomena, in combination with various LR configurations. Luible and Schärer [30] also explored, via full-scale experiments and FE analyses, the LTB performance of glass beams (both monolithic and laminated) with discrete mechanical lateral restraints. The chosen geometrical configuration for the connectors in use (i.e., eight special round aluminum devices, glued to the edge of glass specimens), however, was associated with a mostly rigid and continuous LR effect. The actual contribution and the potential of local restraints for glass beams in LTB were also preliminary explored in [31].

In this paper, the elastic critical buckling moment of LR glass beams in LTB is investigated, with careful consideration of the effects of discrete mechanical restraints (i.e., Figure 2). As known, the knowledge of critical buckling loads for load-bearing systems generally represents poor information for accurate design purposes. Often, however, the availability of simplified (but accurate) calculation approaches can offer robust support to designers. Moreover, the accurate estimation of the expected critical buckling loads represents a key design step toward the definition (or calibration) of standardized calculation procedures and recommendations of practical use [25]. To this aim, extended parametric analytical and FE numerical calculations are presented in this paper, for a wide set of geometrical and mechanical configurations of technical interest. The major advantage is preliminary derived from analytical methods of the literature [32,33], as well as from the LTBeam software [34] (even specifically developed for LR steel members). The LTB performance of LR glass beams having different geometrical features and their sensitivity to variations in the number and position of discrete mechanical restraints are, thus, assessed. More extended parametric calculations are, thus, carried out with the support of ABAQUS software [35], so as to allow for a more refined and/or generalized description of the typical LR configurations in the field of structural glass applications.

To this aim, Section 2 firstly summarizes the current approach for the LTB design of LU glass members. In Section 3, the reference (steel-related) calculation methods are described. In Section 4, the attention is focused on the characterization of selected point fixings in use for glass applications, giving evidence of the expected stiffness parameters and the reliability of simplified, spring-based methods. Finally, Sections 5 and 6 summarize the major outcomes of the extended parametric calculations for LR glass members.

2. LTB Design of Structural Glass Beams

2.1. General Approach for Laterally Unrestrained (LU) Beams

For most existing design standards, guidelines, and regulations for structural beams in LTB, the reference calculation methodology assumes that the member to verify is laterally unrestrained (LU), with fork-torsional end supports (Figure 3). The possible effects due to adjacent or interconnected

constructional members (i.e., roof panels, etc.) are, hence, fully disregarded, in favor of an LTB verification of independent members.

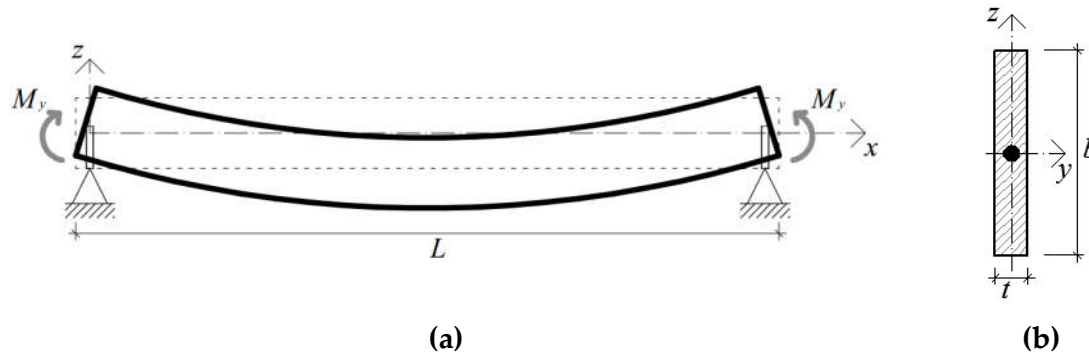


Figure 3. Lateral-torsional buckling (LTB) reference system for a laterally unrestrained (LU) monolithic beam under constant bending moment M_y : (a) front view and (b) nominal cross-section.

Based on literature studies and international design standards for steel structures [36], buckling failure phenomena of structural members according to Figure 3 can be conventionally prevented by means of standardized empirical verification methods, which, in most cases, are developed on standardized design buckling curves. The effective LTB design resistance $M_{b,Rd}$ of the member in Figure 3 can be in fact estimated so as to satisfy the following limit condition:

$$M_{b,Rd} = \chi_{LT} \frac{W_y f_{yk}}{\gamma_{M1}} \geq M_{y,Ed}, \quad (1)$$

where $M_{y,Ed}$ is the design bending moment, W_y is the elastic resistant modulus for the $t \times b$ resisting cross-section, f_{yk} is the ultimate (tensile) resisting stress, and γ_M is a material partial safety factor.

A key input parameter in Equation (1) is represented by the buckling reduction coefficient χ_{LT} ($\chi_{LT} \leq 1$) and, thus, by the normalized slenderness ratio of the structural member to verify.

$$\bar{\lambda}_{LT} = \sqrt{\frac{W_y f_{yk}}{M_{cr}^{(E)}}}, \quad (2)$$

with

$$M_{cr}^{(E)} = M_{cr,0} = \frac{n\pi^2 E I_z}{L^2} \sqrt{\frac{I_w}{I_z} + \frac{L^2 G I_t}{\pi^2 E I_z}}, \quad (3)$$

Euler's theoretical buckling moment.

In Equation (3), E and G denote the Young's and shear moduli, respectively, I_z signifies the moment of inertia about the minor z -axis, and I_t is the torsional moment of inertia for the monolithic $t \times b$ cross-section, with I_w being its warping stiffness (where $I_w \rightarrow 0$ for rectangular cross-sections). At the same time, $n = 1$ is the integer value able to minimize—for a general set of geometrical and mechanical properties—the expected $M_{cr,0}$ value.

As long as Equations (2) and (3) are known, the required buckling reduction coefficient in Equation (1) is given by

$$\chi_{LT} = \frac{1}{\varphi_{LT} + \sqrt{\varphi_{LT}^2 - \bar{\lambda}_{LT}^2}} \leq 1. \quad (4)$$

The latter equation, as known, is sensitive to several aspects, such as $\bar{\lambda}_{LT}$, as well as to the amplitude of initial geometrical imperfections, to the effects of possible residual stresses, and/or to load eccentricities. In Equation (4), all these initial defects are conventionally accounted for as

$$\varphi_{LT} = 0.5 \left[1 + \alpha_{imp} (\bar{\lambda}_{LT} - \alpha_0) + \bar{\lambda}_{LT}^2 \right], \quad (5)$$

where α_{imp} and α_0 are appropriate imperfection factors (see [36] for the reference values in use for steel sections).

In similarity to LU steel members in LTB, design buckling curves were proposed in [25] for LU beams composed of glass. In particular, assuming the characteristic bending tensile resistance of glass $f_{yk} = \sigma_{Rk}$ in (Equation (1)), with $\gamma_M = 1.4$, it was shown in [25] that reliable LTB calculations can be carried out as long as the above imperfection factors are set to $\alpha_{imp} = 0.45$ and $\alpha_0 = 0.20$ (for equivalent initial sine-shaped imperfections of maximum amplitude, $u_{0,max} = L/400$). As long as the design constant bending moment $M_{y,Ed}$ in Equation (1) is replaced by a mid-span concentrated load F or a uniformly distributed load q , the same design approach can still be adopted for glass members in LTB [25]. The standardized verification method is also implemented—with appropriate safety factors—in the set of design recommendations provided in [5] for glass structures. The basic assumption of the design approach is schematized in Figure 4.

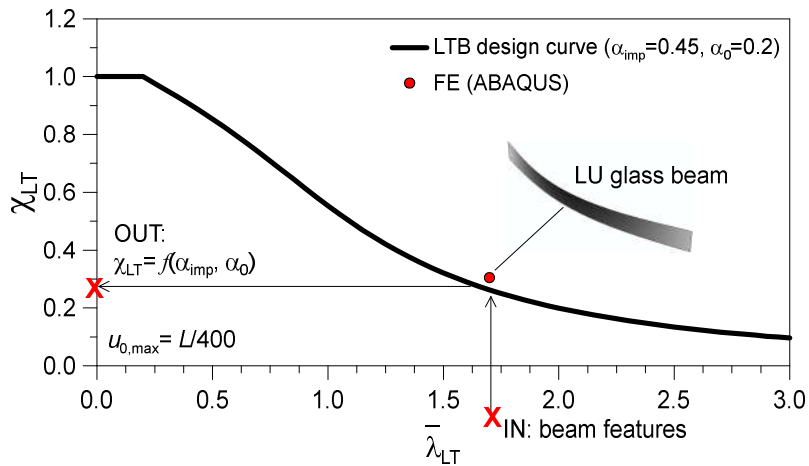


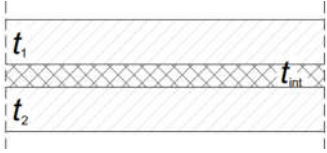
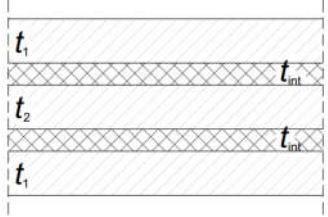
Figure 4. Standardized LTB design approach proposed in [25] for LU glass beams (with $u_{0,max} = L/400$, the maximum amplitude of the reference sine-shaped imperfection).

Worthy of interest is that the above LTB verification approach can be practically extended to laminated glass sections, by accounting for the viscoelastic foils (under well-defined time/temperature conditions) via an equivalent secant shear modulus G_{int} [37-39]. A key step, however, is represented by the reliable calculation of the section properties (especially I_z and I_t). Among others, the equivalent glass thickness t_{eq} can be derived from Table 1; Table 2 (with t_1 , t_2 and t_{int} representing the thicknesses of glass and interlayers).

Table 1. Flexural equivalent section properties for laminated glass beams in LTB, according to [25].

	2 glass layers	3 glass layers
t_{eq}	$\sqrt[3]{t_1^3 + t_2^3 + 12\Gamma_b J_s}$	$\sqrt[3]{2t_1^3 + t_2^3 + 12\Gamma_b J_s}$
I_z	$bt_{eq}^3/12$	
Γ_b	$0 \leq \frac{1}{1 + \pi^2 \frac{E t_1 t_2 t_{int}}{(t_1 + t_2) G_{int} L^2}} \leq 1$	$0 \leq \frac{1}{1 + \pi^2 \frac{E t_1 t_{int}}{4 G_{int} L^2}} \leq 1$
J_s	$t_1(0.5t_1 + 0.5t_{int})^2 + t_2(0.5t_2 + 0.5t_{int})^2$	$t_1(0.5t_1 + 0.5t_2 + t_{int})^2$

Table 2. Torsional equivalent section properties for laminated glass members, according to [25].

	2 glass layers	3 glass layers
		
I_t	$I_{t,1} + I_{t,2} + I_{t,int}$	$2I_{t,1} + I_{t,2} + I_{t,int}$
$I_{t,i}$	$bt_i^3/3 \quad (i=1, 2)$	
$I_{t,int}$	$J_{s,LT} \left(1 - \frac{\tanh(0.5 \lambda_{LT} b)}{0.5 \lambda_{LT} b}\right)$	
$J_{s,LT}$	$4b \frac{t_1 t_2}{t_1 + t_2} (0.5t_1 + 0.5t_2 + t_{int})^2$	$4b \frac{t_1 t_2}{t_1 + t_2} (t_1 + t_2 + 2t_{int})^2$
λ_{LT}	$\sqrt{\frac{G_{int} t_1 + t_2}{G t_1 t_2 t_{int}}}$	$\sqrt{\frac{G_{int} 2t_1 + t_2}{G 4t_1 t_2 t_{int}}}$

2.2. Laterally Restrained Beams with Continuous Adhesive Connections

As long as the glass beam in Figure 3 is characterized by the presence of lateral restraints agreeing with Figure 5a, more accurate calculation approaches are required for reliable predictions. From a mechanical point of view, the resisting cross-section for the LR member in LTB is schematized in Figure 5b.

It was shown in [27–29] that adhesive joints in use for structural glass applications are typically associated with limited stiffness parameters. The presence of (even weak) continuous flexible joints according to Figure 5a, however, can have marked effects on the actual LTB response of a given glass beam. Compared to a basic LU member, the response of the LR element is in fact associated with a modified buckled shape, which can further modify the number of half sine-waves, as long as the adhesive linear restraints are progressively able to prevent possible lateral deformations [27–29].

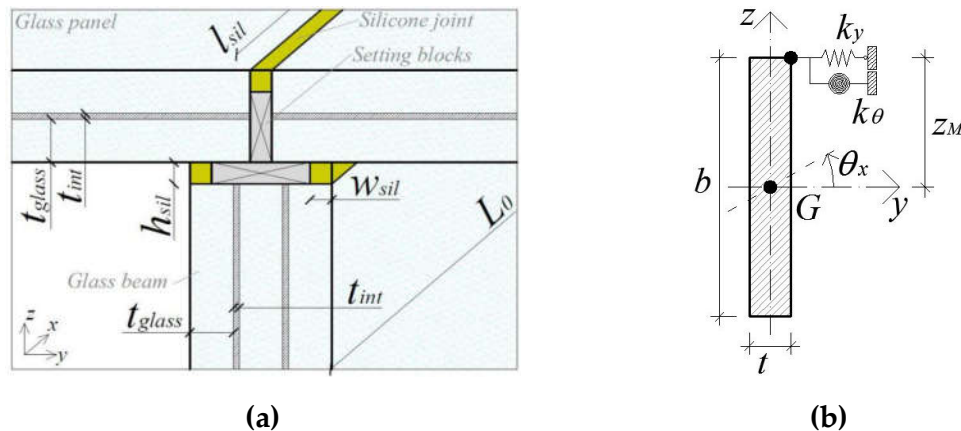


Figure 5. LR glass beams with continuous flexible lateral restraints: (a) example of a beam-to-plate adhesive joint, in accordance with [27], and (b) reference cross-section. Figures reproduced from [27] with permission from Elsevier, Copyright© license number 4813131416995, April 2020.

In terms of LTB design procedure, the presence of the continuous adhesive restraint in Figure 5 manifests in the increase of the critical buckling moment $M_{cr,R} \geq M_{cr,0}$ (with “R” denoting the presence of lateral restraints), as well as in a modification of the fundamental buckling shape,

compared to Figure 4. Given the shear stiffness contribution k_y of the linear restraint (with $k_\theta = 0$), it was, thus, proven in [27] that $M_{cr,R}$ for a general cross-section can be reliably calculated as

$$M_{cr,R} = z_M k_y \left(\frac{L}{n_R \pi}\right)^2 + \sqrt{\left[EI_z \left(\frac{n_R \pi}{L_0}\right)^2 + k_y \left(\frac{L}{n_R \pi}\right)^2 \right] \left[EI_w \left(\frac{n_R \pi}{L}\right)^2 + GI_t + z_M^2 k_y \left(\frac{L}{n_R \pi}\right)^2 \right]}, \quad (6)$$

where $n_R \geq 1$ is the integer number of half-sine waves able to minimize Equation (6), while z_M is the distance between the lateral restraint and the longitudinal axis of the beam (Figure 5b).

It is important to note that, as long as $M_{cr,R}$ is modified in Equation (6), the normalized slenderness ratio $\bar{\lambda}_{LT}$ in Equation (2) is also modified. Accordingly, the susceptibility of a given LR glass member to LTB phenomena (i.e., Equation (4)) can be reasonably different from that of an identical LU geometry. In any case, it was shown in [27] that Equations (1)–(5) and Figure 4 can be still adopted for LTB design purposes, as long as the actual $M_{cr,R}$ value is properly estimated (Equation (6)) and possible global imperfections for the element to verify do not exceed the reference equivalent amplitude ($u_{0,max} = L/400$).

2.3. Laterally Restrained Beams with Discrete Mechanical Connections

When discrete mechanical restraints according to Figures 2 or 6 are used for glass beams, further design issues must be unavoidably assessed, compared to Sections 2.1 and 2.2.

The actual role and LTB efficiency of discrete restraints agreeing with Figure 6a (that could be variably spaced and positioned along the span of a glass member) should in fact be properly characterized. Under ordinary design loads, moreover, major calculation troubles for resistance verifications may usually derive from the presence of glass holes, which should respect appropriate geometrical prescriptions (Figure 6b). In the multitude of mechanical devices that are commercially available for structural glass applications, the goal of design practice is, in fact, to avoid premature cracks in glass, as well as to facilitate the installation stage. Stiff metal connectors agreeing with Figure 6a, as such, generally use soft layers and gaskets that are interposed to the edges of glass, in order to accommodate local relative displacements and to protect the edges from potential stress peaks. From an LTB calculation perspective, all the above aspects manifest in the form of additional local stiffness (of devices) and flexibility (due to gaps/gaskets) that should be properly taken into account, even for the prediction of the theoretical critical buckling moment $M_{cr,R}$.

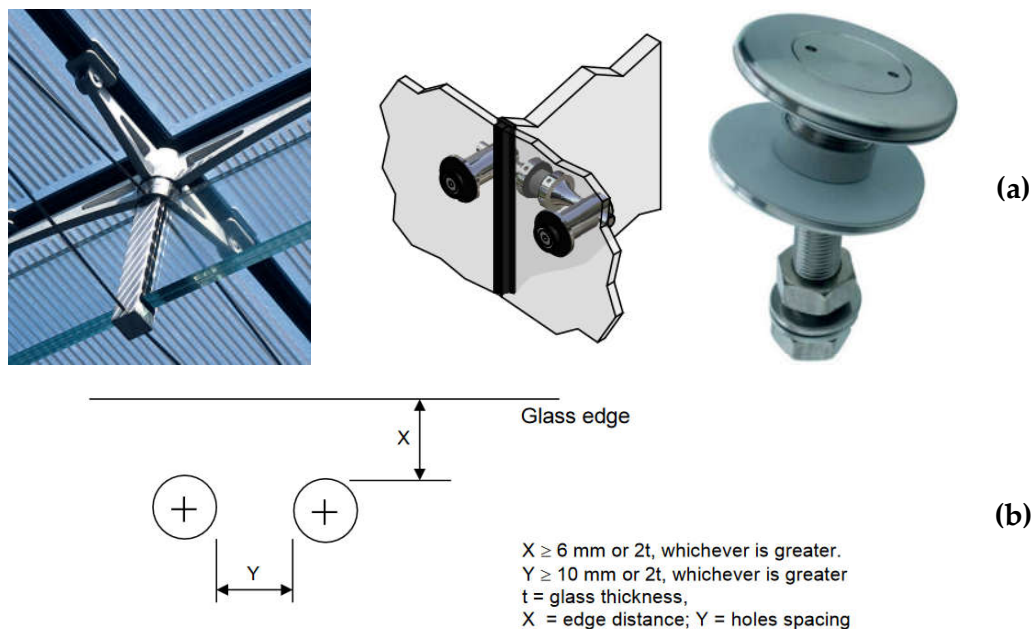


Figure 6. LR glass beams with discrete mechanical lateral restraints: (a) examples of point fixings and (b) schematic representation of minimum distance requirements for the glass holes.

3. LTB Theoretical Background and Solving Methods for LR beams with Discrete Mechanical Restraints

In the last few decades, several research projects focused on the LTB analysis of (non-glass) load-bearing members with discrete mechanical restraints. Most efforts were specifically aimed at steel load-bearing systems, offering accurate theoretical formulations and simplified analytical approaches in support of designers [32, 33, 40–42]. A brief overview of suitable methods is proposed in this section.

Among the available calculation tools that could be extended to LR glass members in LTB, the first issue is related to the accurate prediction of the theoretical critical moment $M_{cr,R}$. In addition to the basic variations in the intrinsic material properties, compared to steel girders, glass beams are in fact expected to have relatively higher length-to-thickness and length-to-height ratios, thus further enforcing their susceptibility to possible LTB phenomena. Further key parameters to account for in LTB calculations of LR glass members are then represented by the following mechanical restraints in use (*rotules*, etc.).

- their number (generally $n_b > 1$),
- the spacing s and position (with the respect of minimum edge-distance of glass holes, etc.),
- the detailing features, for devices that are specifically designed for glass applications (i.e., Figure 6),
- finally, the presence of gaps and soft gaskets at the glass-to-restraint interface, as typically in use to prevent local stress peaks in the region of holes.

3.1. Reference Theoretical Formulation for I-section Steel Beams

Extended studies for the LTB analysis of steel beams with discrete restraints were carried out in [32, 33]. Following Figure 7, the critical buckling moment of a simply supported, doubly symmetric I-section steel beam with span L and a number n_b of discrete, elastic lateral restraints (with infinitely rigid stiffness K) is generally recognized to be

$$M_{cr,R} = M_T = \frac{\pi^2 EI_z}{s^2} \sqrt{\frac{I_w}{I_z} + \frac{s^2 GI_t}{\pi^2 EI_z}}, \quad (7)$$

where Equation (8),

$$s = \frac{L}{n_b + 1}, \quad (8)$$

denotes the uniform distance of the n_b discrete restraints; thus, Equation (9),

$$M_{cr,R} = (n_b + 1) \cdot M_{cr,0}, \quad (9)$$

is the upper theoretical limit for the expected buckling resistance, compared to Equation (3).

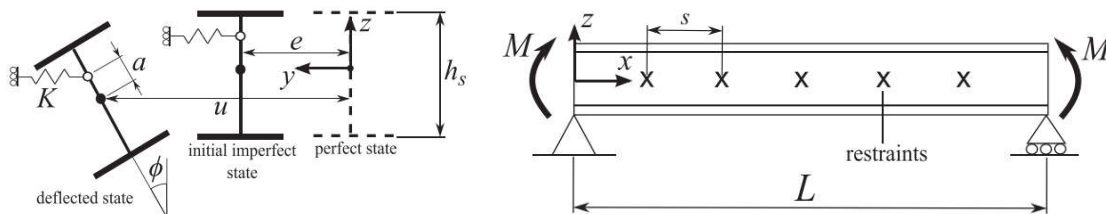


Figure 7. Reference analytical model for LR beams with discrete rigid lateral restraints. Figure adapted from [33] with permission from Elsevier, copyright© license number 4813141188013, April 2020.

The above formulation assumes that the so-called “threshold” moment M_T represents the bending moment for which the LR beam buckles in $(n_b + 1)$ half-sine waves. In other words, the stiffness K of $n_b \geq 1$ restraints is so high that a fully rigid lateral bracing can be offered to the beam to verify, i.e., with null lateral displacements at the locally restrained nodes. As such, the same M_T value is equivalent to the critical moment of an LU beam segment with identical cross-section properties but total span s (see Equation (8)).

Major issues for the LTB analysis of a general steel girder (see [32,33]) are thus represented by the “rigidity efficiency” of the discrete restraints in use and, thus, by the detection of possible intermediate configurations in which certain nodal displacements could be expected in the region of discrete restraints. McCann et al. [33], for example, solved a linear Rayleigh–Ritz analysis and proposed an extended formulation for the LTB analysis of general LR steel beams. According to [33], it was shown that, once K exceeds the “threshold” stiffness value K_T , the lateral restraints in use have a full bracing effect; thus, Equation (10),

$$K \geq K_T, \quad (10)$$

reflects a critical buckling moment $M_{cr,R}$ agreeing with Equation (7). To this aim, the threshold stiffness value must be estimated as

$$K_T = \left(\frac{EI_z}{s^3} \right) \frac{62 (1 + \kappa_s)}{A_0 + A_1 \hat{a}}, \quad (11)$$

with the equations below denoting the normalized distance between the discrete restraints and the section shear center (with h_s representing the total height of the I-shaped profile in Figure 7).

$$\kappa_s = \frac{\kappa}{(n_b + 1)^2}, \quad (12)$$

$$\kappa = \frac{L G I_k}{\pi^2 E I_w}, \quad (13)$$

$$a^* = \frac{2a}{h_s}, \quad (14)$$

Finally, according to [33],

$$A_0 = 0.45 + 2.8 v_{b,T} \kappa_s, \quad (15)$$

$$A_1 = 6.3 v_{b,T} + 2.2 \kappa_s - 1, \quad (16)$$

$$v_{b,T} = \frac{1}{1 + \cos[(\pi/n_b + 1)]}. \quad (17)$$

More in detail, $v_{b,T}$ in Equation (17) is respectively equal to 1.0 for $n_b = 1$, 0.667 for $n_b = 2$, and 0.586 for $n_b = 3$, while it tends progressively to the lower limit $v_{b,T} = 0.5$ for higher n_b values.

Following Figure 7, a key condition for Equations (7)–(17) is that the discrete restraints in use are positioned at a height a above the shear center of the cross-section object of analysis (with positive distance values for bracing systems on the compression side), such that the following equation applies [33]:

$$a \geq a_{\text{lim}} = \frac{h_s + \kappa_s}{4\sqrt{1 + \kappa_s}} \quad (18)$$

3.2. Linear Interpolation Approaches

According to Equation (7), it is rationally expected that the critical buckling moment of a given LR member in LTB can increase significantly, as long as rigid lateral restraints (with $n_b \geq 1$ and $s < L$) are able to prevent possible displacements of the involved nodes. At the same time (see Equations (7)

and (9)), $M_{cr,R}$ progressively decreases for $K < K_T$, and finally returns to the limit condition represented by the LTB response of a simple LU beam (see Equation (3)).

Several research studies were carried out over the years for the LTB assessment of LR steel girders, where relatively stiff purlins of other bracing systems were used to provide stabilization. Major calculation troubles arise when node-displacing critical modes can occur, since closed-form solutions cannot be analytically derived for the reliable prediction of the critical moment $M_{cr,R}$. McCann et al. [33], in this context, proposed a conservative, linear approximation for intermediate stiffnesses (i.e., $0 < K < K_T$), so that the corresponding $M_{cr,R}$ value could be reliably estimated as

$$M_{cr,R} = M_{cr,0} + \frac{K}{K_T}(M_T - M_{cr,0}), \quad (19)$$

with $M_{cr,0}$ and M_T representing the unrestrained and threshold critical values given by Equations (3) and (7), respectively. Past comparative calculations and validation studies discussed in [32,33] proved that Equation (19) can be suitable for the LTB design of general steel beams. However, the same studies highlighted that a higher degree of accuracy can be expected, especially for steel members with a braced compression flange and with a single restraint ($n_b = 1$) at the mid-span section.

An alternative linear fitting approach was suggested by Trahair [43], for LR beams with a single restraint ($n_b = 1$). The latter, however, can be applied with accuracy to beams with a discrete restraint on the shear center (i.e., $a^* = 0$ in Equation (14)). Many other approximation proposals are also available in the literature, and they are specifically validated for a given number, position, and stiffness of discrete restraints in steel members. Parametric studies were discussed in [42], for steel members under various loading and LR conditions of technical interest for design. Extended parametric analyses were presented in [29] for steel beams under various LR configurations, but giving evidence of the intrinsic advantages or limits for several linear interpolation approaches of the literature.

In this research paper, parametric calculations are, thus, proposed for several LR glass members in LTB. As a reference toward more refined calculations, the linear interpolation approach in Equation (19) is taken into account.

3.3. LTBeam Tool for Steel Beams

The LTBeam tool is firstly considered as an alternative calculation method. The software, more in detail, was developed at CTICM (Centre Technique Industriel de la Construction Metallique, www.cticm.com [34]), as part of a past European research project. The original goal of this tool is to compute the elastic critical moment $M_{cr,R}$ of LR steel beams with general cross-sectional features, in any number of different load cases and boundaries, according to the finite element (FE) method.

For a given cross-section (both mono- or double-symmetric), the assigned beam to verify is discretized into a maximum of 300 FE elements. Non-steel members can also be efficiently investigated, once the flexural, torsional, and warping cross-section properties are defined in the input parameters, together with the Young's modulus and Poisson's ratio for the material in use. The presence of LR mechanical restraints (up to $n_b = 2$), finally, can be described in the form of equivalent elastic springs with input stiffness and position. When alternative calculation methods are not available, an intrinsic advantage of the LTBeam tool is that the expected K_T value in Equation (19) can be numerically derived by iteration, i.e., as the minimum stiffness K that leads $M_{cr,R}$ to coincide with the threshold critical moment M_T for the member object of analysis.

3.4. General FE Numerical Method

When the input geometrical details for the system to verify do not match with the approaches summarized in Sections 3.2 and 3.3, commercially available computer software codes can be adapted to specific configurations.

In this paper, for example, a set of parametric linear buckling analyses were developed with the ABAQUS/Standard software ("buckle-linear perturbation" step). Through the parametric investigation, the same modeling technique was taken into account to describe various LTB

configurations characterized by different number, position, and stiffness of discrete restraints, among a wide series of beam geometries. The typical FE model consisted of S4R four-node, quadrilateral, stress/displacement shell elements with reduced integration and large-strain formulation (S4R type of ABAQUS element library; see Figure 8a). A regular mesh pattern was used, with l_{mesh} , the characteristic size of quadrilateral elements, comprised between 2 mm and 5 mm, depending on the global dimensions $b \times L$ of the studied beams. Given the goal of linear bifurcation analyses, glass was described as an isotropic, indefinitely linear elastic material.

Boundary conditions for the simply supported, fork-end supported beams in LTB were described via equivalent nodal constraints, so as to reproduce the reference set-up in Figure 3. Restraints were used for both the shear center of the beam end sections ($u_y = 0, u_z = 0$), and all the end section nodes ($u_y = 0$), as shown in Figure 8b. Accordingly, bending moments M_y were introduced at the barycentric node of the end sections in Figure 8. A “coupling” kinematic constraint was used to redistribute the so-defined bending moments on the section height b .

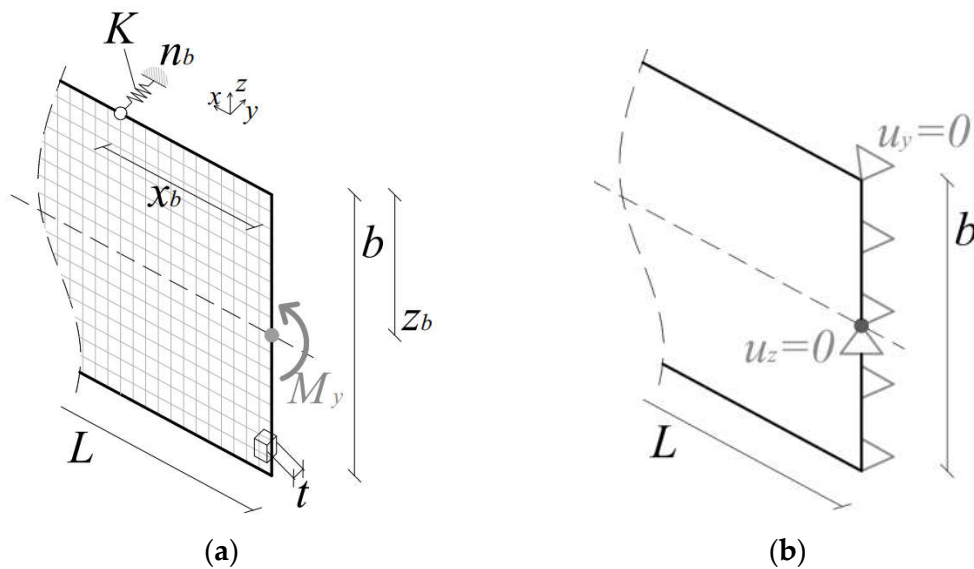


Figure 8. Preliminary finite element (FE) numerical model for linear bifurcation analyses on LR glass beams in LTB (ABAQUS).

According to several literature contributions on LR steel members in LTB, the bracing effect of discrete mechanical restraints was numerically reproduced in a simplified way, i.e., by means of a number n_b of linear elastic springs (“axial” type) with stiffness K . These springs were introduced to brace the compression edge of the examined glass beams, at a given distance z_b from the shear center. Single restraints ($n_b = 1$) were placed at the mid-span section of the selected geometries ($x_b = L/2$). In presence of multiple restraints ($n_b > 1$), an equal spacing s was taken into account (Equation (8)). The detailing of holes in glass, finally, was disregarded for the elastic LTB analysis of the so-assembled spring-based models.

4. Mechanical Characterization of LR Glass Beams with Discrete Restraints

4.1. Design Issues

When the calculation approaches summarized in Section 3 are taken into account for LTB calculations, an open issue for glass members is certainly related to the actual effects of real mechanical restraints. According to Figure 6, most of them are in fact characterized by geometrical and mechanical features that often hardly match with idealized nodal elastic springs.

As such, a preliminary attempt of this project was, thus, dedicated to the assessment of nominal features for some of the discrete restraints that are actually used for structural glass fins in roofs and

facades. In addition to the multitude of commercially available solutions, the attention was focused on the selected configuration in Figure 9. The latter includes a stainless-steel device (AISI 316 alloy type) and is intended for glass fins up to 19 mm in total thickness. Two 100-mm-spaced holes are used to fix the steel plates to the glass section. Two lateral rigid bars for the spider device allow then the connection between the glass fin and the orthogonal plates (point fixing *rotules*). To avoid local stress peaks in glass, Teflon® (polytetrafluoroethylene, PTFE) washers are interposed onto the glass beam and the metal components. Such a design solution is in line with the point fixing practice of glass structures, where various low-modulus soft layers can be used. Possible alternatives involve nylon, polyoxymethylene (POM), ethylene propylene diene monomer (EPDM), or other rubber materials [1]. Dedicated studies, accordingly, should be generally spent for the characterization of different restraint solutions. Usually, the above details result from accurate design and resistance verification steps [1]. Given that the low-modulus materials in use can be sensitive to time loading and temperature, their mechanical properties should be properly assessed, with the support of literature documents or experiments [44–49]. For preliminary LTB estimates, however, these soft layer properties can be assumed as equivalent linear elastic terms.

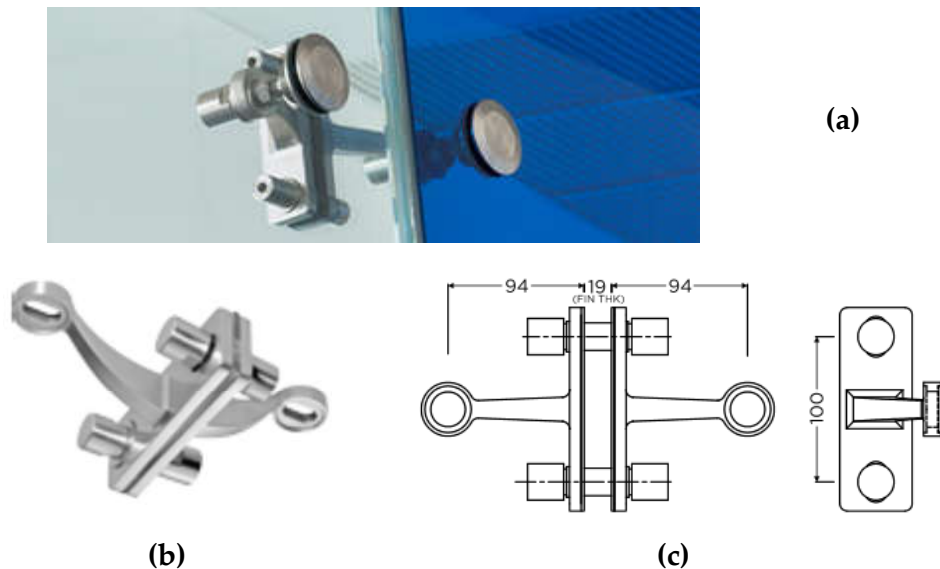


Figure 9. Example of two-way spider mechanical restraint for glass members: (a) global assembly with rotules; (b) axonometry detail; (c) nominal dimensions (top and side views, values in mm).

4.2. FE Buckling Analysis and Stiffness Estimate for LR Glass Members

To solve the above issue and assess the reliability of simplified spring-based FE calculations, the modeling approach described in Section 3.4 was, thus, further elaborated to include a more refined description of restraint details. The example in Figure 10, in particular, was developed by taking inspiration from Figure 9. From a mechanical point of view, the latter represents a single discrete restraint ($m_b = 1$) composed of two point fixings ($n_a = 2$) with a certain local stiffness K_a .

For the FE analysis, a set of solid brick elements were, thus, used to reproduce the device components. The materials in use (glass and steel) were described via linear elastic constitutive laws, with $E = 70$ GPa, $\nu = 0.23$ for glass [50] and $E_s = 197$ GPa, $\nu_s = 0.3$ for steel [51]. Two spider plates similar to Figure 9 were firstly introduced in the FE assembly (see Figure 10a). The 100-mm-spaced bolts were reproduced via kinematic constraints (“beam MPC” option from the ABAQUS library) able to offer a rigid axial and rotational restraint to the involved opposite faces, in the region of holes (see the detail “A” in Figure 10a). At the same time, a frictionless surface contact interaction was interposed at the adjacent glass-to-steel surfaces (i.e., where soft, frictionless gasket layers are used).

The lateral rigid bars of the spider device in Figure 9, finally, were schematized in the form of squared-shape geometries. Compared to the nominal device in Figure 9, an average cross-sectional

area was taken into account, given that the length and height of these bars was respected. Above these bars (see the detail “B” in Figure 10a), two point fixings were in fact introduced in the form of solid discs. For each one of them, the middle axis was placed at a distance of 94 mm from the external face of the beam. The steel plates and the corresponding lateral bars were ideally “tied”, thus enabling possible relative deformations.

Special care was dedicated to the description of the mechanical interaction between the spacer bars and the above point fixings. To this aim, a combined “axial + rotational” connector was introduced between each spider bar and the corresponding top plate (detail “B” of Figure 10a). Such an assumption was chosen to characterize the nominal geometrical detail in Figure 10b, where the device and the glass hole (of the braced orthogonal glass plate) must interact via the interposed gap and soft gasket. The schematic drawing in Figure 10b, in this regard, adequately reproduces the theoretical behavior for the examined point fixing detail and a given glass beam in LTB. The connector, as usual, does not react in tension. Otherwise, on the compression side, it is expected to progressively enable possible lateral displacements of the beam. At first, the assigned gap allows a certain accommodation of local deformations ($K_d = 0$). When the contact initiates between the bolt device and the adjacent soft layer, a certain stiffness K_d is indeed offered against possible lateral deformations of the beam. This local stiffness contribution, however, could be susceptible to local crushing of the soft layer, thus requiring specific design of geometrical details.

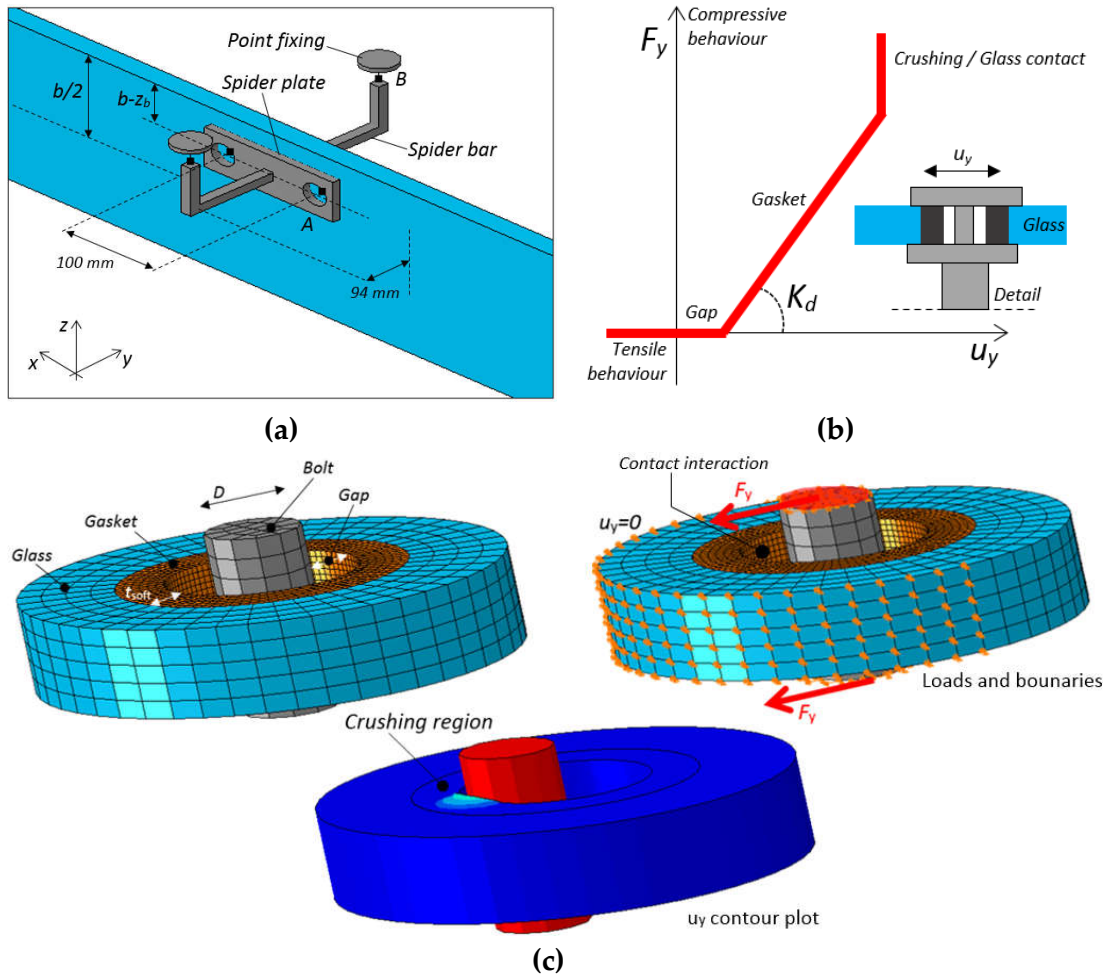


Figure 10. FE numerical modeling of glass beam in LTB ($m_b = 1$, $x_b = L/2$): (a) restraint detail, with evidence of (b) mechanical characterization of gaskets (detail “B”), and with (c) example of local FE model for the stiffness analysis of a “detail B” point-fixing (ABAQUS).

The reliable calculation of $M_{cr,R}$ for a given LR member, according to Section 3, requires that the global elastic stiffness K for the spider device should be estimated first.

For practical LTB calculations, it is assumed that each detail agreeing with Figures 10a,b (where $n_b = 1$ and $n_d = 2$) is the result of multiple local stiffness contributions K_d (if $n_d > 1$) that can be placed at different x_b positions of the span L for the LR beam to verify. The cumulative stiffness K due to the mechanical restraint in Figure 10 is, thus, expected to be

$$K = \sum_{d=1}^{n_d} K_d, \quad (20)$$

where Equation (21),

$$K_d = \frac{F_y}{u_y}, \quad (21)$$

represents the equivalent stiffness for a single point fixing. The latter depends on the Young's modulus of the soft layer in use (E_{soft}), its thickness t_{soft} , and the contact surface in compression (A_{soft}), in the region of interaction between the bolt and the glass hole. Accordingly, dedicated experimental analyses or refined FE calculations should support the accurate characterization of local mechanical behaviors (Figure 10c). As long as the calculations are limited to the linear elastic regime, however, an approximate prediction of this local stiffness K_d can be obtained as

$$K_d \approx \frac{E_{soft} A_{soft}}{t_{soft}}, \quad (22)$$

with

$$A_{soft} \approx t_{soft} 0.8D, \quad (23)$$

and D the nominal diameter of the bolt.

It is, thus, clear that, as long as the input parameters in Equations (22) and (23) are modified, a markedly different prediction can be achieved for the total stiffness K in Equation (20). The latter, in addition, can have different bracing effects and efficiency, depending on the geometry of the LR beam to verify.

The example in Figure 11, in this regard, shows the typical deformed shape for a selected geometry ($t = 20\text{mm}$, $b = 200\text{mm}$, $L = 2000\text{mm}$) and a single LR device according to Figure 10a ($n_b = 1$, $n_d = 2$, $x_b = L/2$, $z_b = 55\text{mm}$). The deformed shape in Figure 11 specifically refers to a total elastic stiffness $K = 40\text{ kN/m}$ (with $K_T = 144\text{ kN/m}$, $M_{cr,0} = 18.69\text{ kNm}$ and $M_T = 37.38\text{ kNm}$).

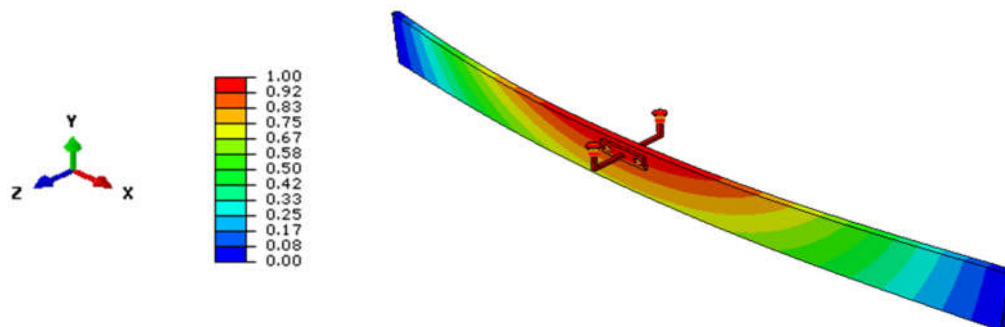


Figure 11. Example of fundamental critical shape (ABAQUS) for a glass beam in LTB ($n_b = 1$, $x_b = L/2$) with LR details according to Figure 10.

From the deformed shape in Figure 11 (weak restraint), it is possible to notice that the spider device does not affect the global LTB response of the glass beam. In other words, as long as the total stiffness K is limited, compared to K_T , local deformations are still allowed for the restrained nodes.

From Table 3, moreover, it is possible to see the variation of critical moment estimates for the same beam geometry, as long as K increases. The collected values are obtained from the linearized analytical approach, the LTBeam tool, and the refined FE model in Figure 11.

Table 3. Comparison of critical buckling moment variations for the selected beam geometry from Figure 11 ($n_b = 1$ and $n_d = 2$), as a function of K (3D= three-dimensional).

K (kN/m)	$M_{cr,R} / M_{cr,0}$		
	Analytical (Equation (19))	LTBeam (spring-based model)	FE (model with 3D restraints)
40	1.278	1.350	1.383
80	1.554	1.632	1.655
120	1.725	1.870	1.858

As long as K increases, the bracing effect of local restraints manifests in a progressive increase of $M_{cr,R}$, within the limit values $M_{cr,0}$ and M_T . The comparison of analytical, LTBeam, and more refined FE calculations in ABAQUS shows that the first approach tends to underestimate the expected bracing effect, while the general trend of numerical calculations is mostly in good correlation. For the selected example, the spring-based estimates show less than a 2% scatter from the more accurate FE model with three-dimensional (3D) restraints.

A relevant calculation issue is, thus, represented by the threshold stiffness value K_T described in Equation (19), given that Equations (11)–(17) were specifically proposed in [32,33] for doubly symmetric I-section steel members. The reference analytical approach can be further adapted to rectangular $t \times b$ glass sections, as long as it is assumed that the warping stiffness in Equation (13) reduces to

$$I_w \approx I_w^* = \frac{I_z(b^2)}{4} = \frac{b^3 t^3}{48}. \quad (24)$$

Consequently (with $G \approx E/3$ the shear modulus of glass), the original Equation (13) can be expressed as

$$k \approx \frac{16L}{\pi^2 b^2}. \quad (25)$$

Once k is estimated from Equation (25), the final K_T value can, thus, be calculated via Equation (11). Compared to the exact formulation (i.e., Equation (13) or iterative calculations with the LTBeam tool, see Section 3.3), it is important to note that Equation (25) can result in rough threshold stiffness predictions for a given LR glass member. Therefore, careful consideration should be spent, at the design stage, to account for these intrinsic approximations.

In this regard, comparative calculation examples are proposed in Figure 12a for selected LR configurations, while the corresponding percentage scatter ΔK_T (as obtained from Equation (25) or more accurate predictions) is shown in Figure 12b. The latter, given the assumption of Equation (25), can result in both positive or negative scatter (depending on the distance a'), and even in severe scatter. The combination of geometrical properties for the beam to verify, as well as the position of restraints, can both contribute to affect the final K_T result. According to Figure 12c, however, it is possible to see that the approximation in K_T calculated from Equation (25) can be efficiently addressed (for various glass beam geometries and restraint positions), as long as the suggested interpolation function is taken into account.

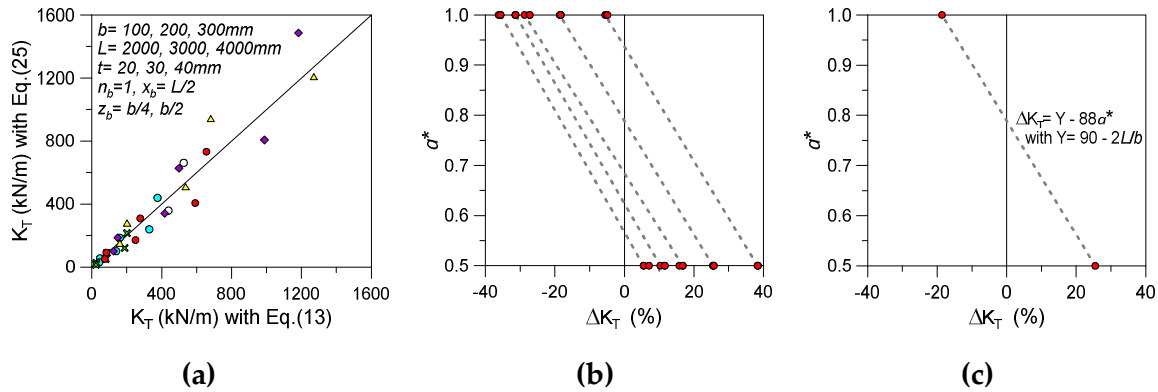


Figure 12. Comparative calculation of threshold stiffness K_T for LR glass beams, with evidence of (a) expected accuracy, (b) corresponding percentage scatter ΔK_T deriving from the adapted calculation approach (Equation (25), with selected results grouped by L/b and a^*), and (c) correction proposal.

5. Analytical and FE Numerical Parametric Investigation

In accordance with Sections 3 and 4, a series of parametric calculations were carried out on a wide set of geometrical and mechanical configurations. The critical buckling moment $M_{cr,R}$ of monolithic glass beams subjected to a constant, positive bending moment M_y agreeing with the set-up in Figure 3 was predicted. Key input variations for the parametric study included modifications of the following:

- span L for the selected glass beams (with $L = 2000, 3000, 4000$ mm),
- cross-sectional dimensions $t \times b$ (with $t = 20, 30, 40$ mm and $b = 100, 200, 300$ mm),
- position z_b of restraints (with $z_b = 0, b/4$, or $b/2$),
- stiffness K of restraints ($K = \text{var}$).

Through the calculation steps, moreover, three different methods were assessed:

- simplified analytical calculations given by the modified linearized approach (i.e., Equation (19), with K_T from Equation (11) and k given by Equation (25) and Figure 12c).
- LTBeam estimates: for each glass member, the equivalent section properties and LR features were considered for the software input,
- FE (ABAQUS) models: based on Section 3.4 and Figure 8, where spring-based, *axial* connectors were used for the description of lateral restraints.

For all the above methods, the Young's modulus of glass was set to $E = 70$ GPa, with $\nu = 0.23$ as the Poisson's ratio [50].

5.1. Stiffness K and Position z_b of Single Discrete Restraints ($n_b = 1$)

A first series of comparative calculations was carried out for glass beams characterized by the presence of a single discrete restraint. Figure 13 shows the typical variation of critical moment $M_{cr,R}$ for a given beam geometry ($t = 20$ mm, $b = 200$ mm, $L = 2000$ mm), as long as K is modified.

Together with the critical buckling moment, as expected, the deformed shape of the beam is progressively modified with K , from a single half-sine wave (weak lateral restraint, $K \rightarrow 0$) toward a double half-sine wave shape that is characterized by null displacements of locally restrained nodes ($K \rightarrow K_T$), as shown in Figure 14. Given that both the geometrical properties of the beam's object of analysis and the restraint features can affect the final LTB predictions, additional calculations were, thus, carried out with the three selected methods earlier defined.

Typical results are reported in Figure 15, in non-dimensional form, where the parameters in Equations (26) and (27),

$$R_M = \frac{M_{cr,R}}{M_{cr,0}}, \tag{26}$$

$$R_K = \frac{K}{K_T}, \tag{27}$$

denote the theoretical resistance increase and the stiffness efficiency for the discrete restraints in use, respectively.

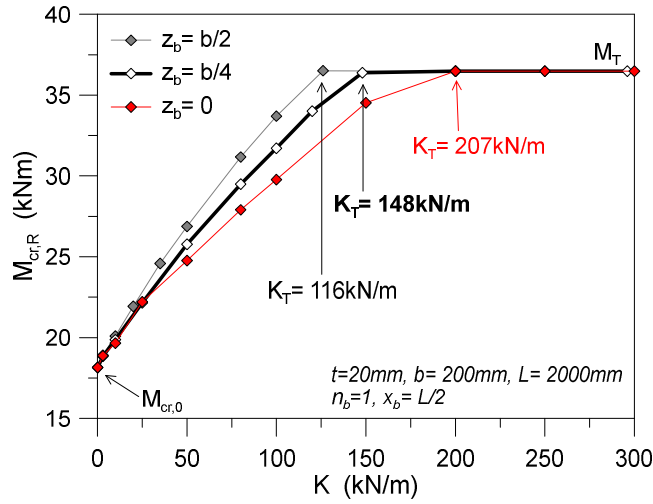


Figure 13. Comparative LTB calculations for selected LR glass beams with $n_b = 1$ discrete lateral restraints at different positions z_b ($K = \text{var}$), using ABAQUS.

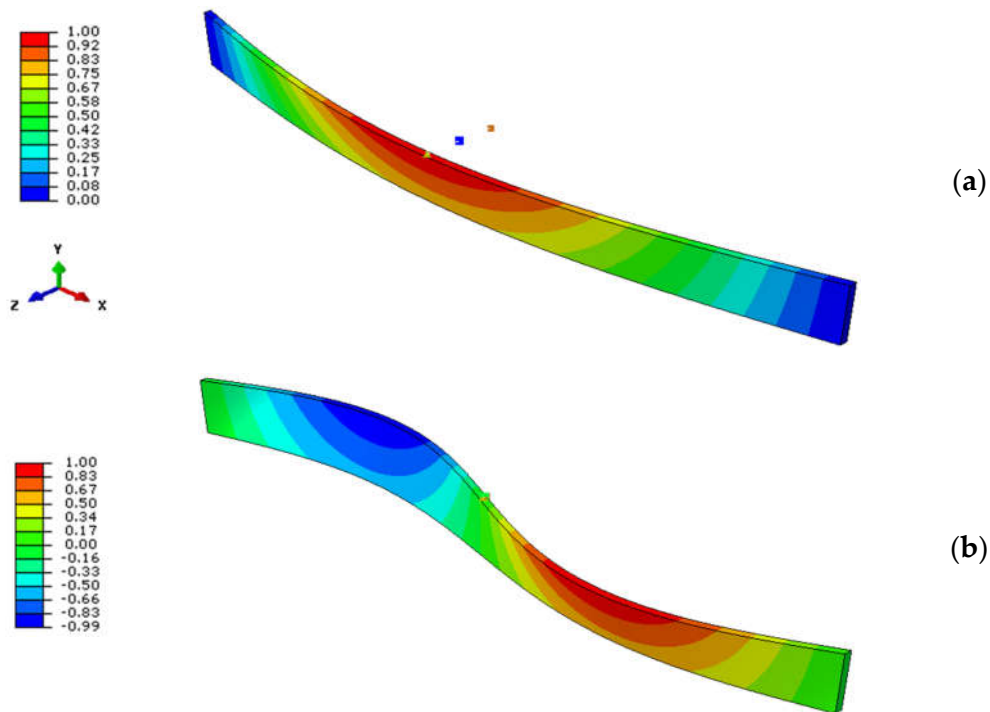


Figure 14. Typical LTB deformed shape for a selected LR glass beam ($L = 2000 \text{ mm}$, $b = 200 \text{ mm}$, $t = 20 \text{ mm}$) with discrete lateral restraints ($n_b = 1$, with $x_b = L/2$ and $z_b = b/2$): (a) example of LU beam ($K \rightarrow 0$) and (b) LR limit condition ($K \rightarrow K_T$), using ABAQUS.

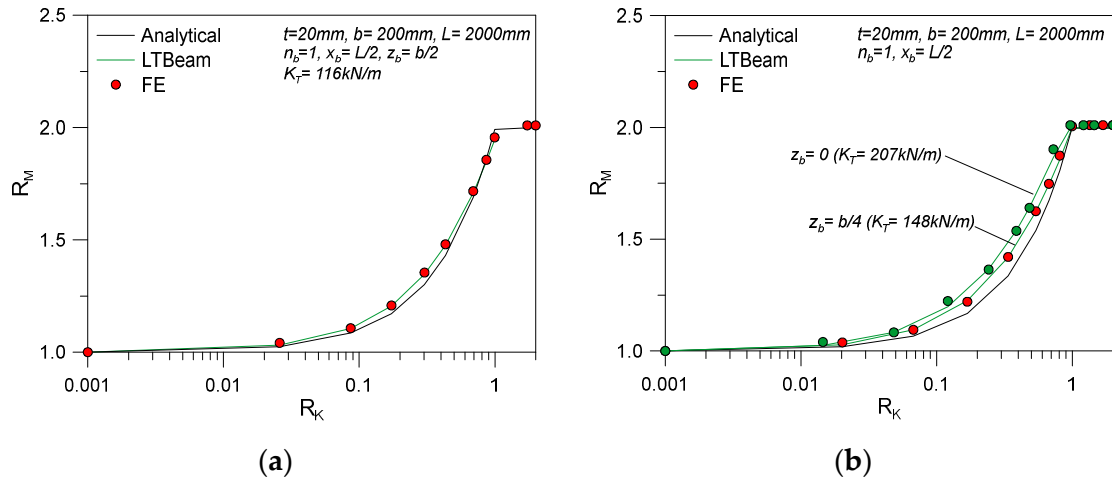


Figure 15. Comparative LTB calculations for LR glass beams with discrete lateral restraints ($n_b = 1$) at different positions z_b ($K = \text{var}$): (a) $z_b = b/2$ and (b) $z_b = 0, b/4$.

Figure 16, finally, presents the major outcomes of an extended analysis carried out on glass beams in LTB with a single discrete restraint ($0 \leq K \leq K_T$). The collected results are compared in the form of R_M values (Equation (26)), as obtained for beam geometries grouped by span ($L = 2000, 3000, 4000$ mm), height ($b = 100, 200, 300$ mm), and thickness ($t = 20, 30, 40$ mm). Possible variations in the position of single restraints from the beam shear center are also taken into account ($z_b = 0, b/4$, or $b/2$, with $x_b = L/2$). When both the beam geometry and the restraint stiffness K are modified, it is interesting to note in Figure 16 a relatively stable trend for the R_M estimates from the numerical software or the “modified” linearized analytical approach.

For a more accurate quantification of the expected percentage scatter due to the intrinsic approximation from the analytical calculations, however, the percentage value in Equation (28) can be taken into account

$$\Delta M_{cr,R} = 100 \cdot \frac{x_{num} - x_{an}}{x_{an}}. \quad (28)$$

According to Figure 17, it is thus possible to note that the linearized analytical predictions are in rather good correlation with more detailed FE methods, for relatively stiff restraints ($K > 0.8K_T$, for the examined systems).

The theoretical buckling moment of the selected LR beams is always underestimated by the linearized approach, as also expected. However, the percentage scatter from Equation (28) is less than 2% for most of the examined configurations. For intermediate K values (see Figure 17), the underestimation of LR bracing effects is maximized in the range of $K = 0.3\text{--}0.4K_T$, with up to 7–8% scatter. As a result, the use of a linear approximated formulation is proven to offer reliable (and not severely conservative) predictions for the critical buckling moments for LR glass beams with single discrete restraints.

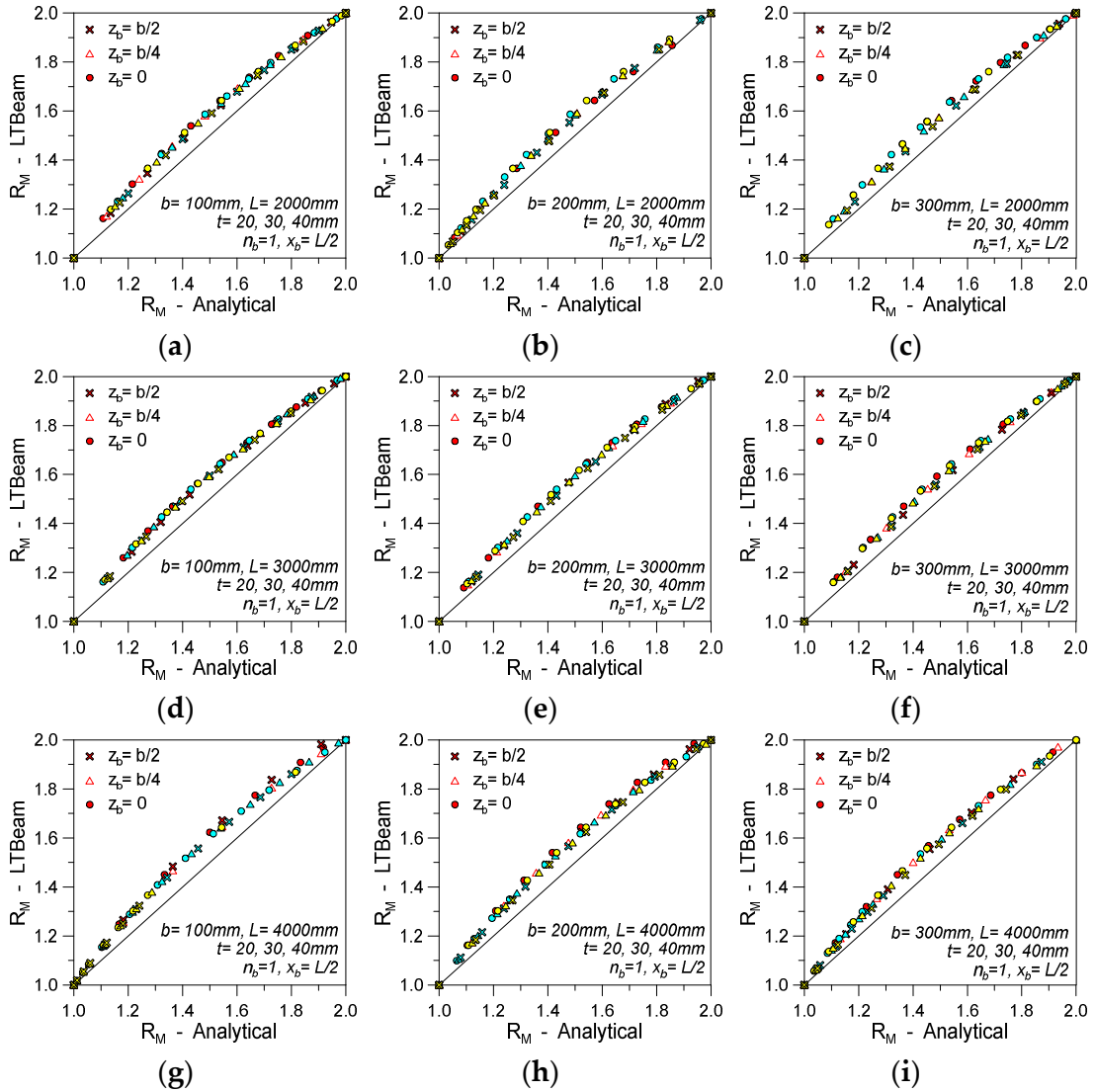


Figure 16. Comparative R_M calculations (Equation (26)) for LR glass beams in LTB ($n_b = 1, K = \text{var}$).

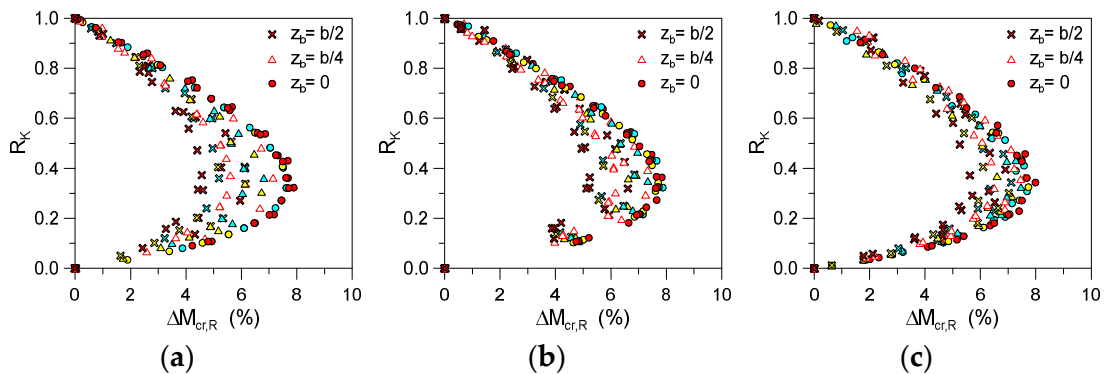


Figure 17. Percentage scatter (Equation (28)) for critical buckling moment estimates of selected LR glass beams ($n_b = 1, K = \text{var}$) grouped by span: (a) $L = 2000$ mm, (b) $L = 3000$ mm, and (c) $L = 4000$ mm (with $t = 20, 30, 40$ mm and $b = 100, 200, 300$ mm).

6. Analysis of Glass Beams with Multiple Discrete Restraints

At a subsequent stage, the parametric analysis was extended to LR glass beams characterized by the presence of multiple discrete restraints. Major results are grouped in Sections 6.1 and 6.2, as a function of n_b (with $2 \leq n_b \leq 5$).

6.1. Two Restraints ($n_b = 2$)

For glass beams with two equally spaced discrete restraints, most of the FE results and analytical calculations were proven to agree with the examples in Figure 18a. Therefore, it is possible to note that the linearized approach has a more pronounced underestimation of the corresponding FE estimates.

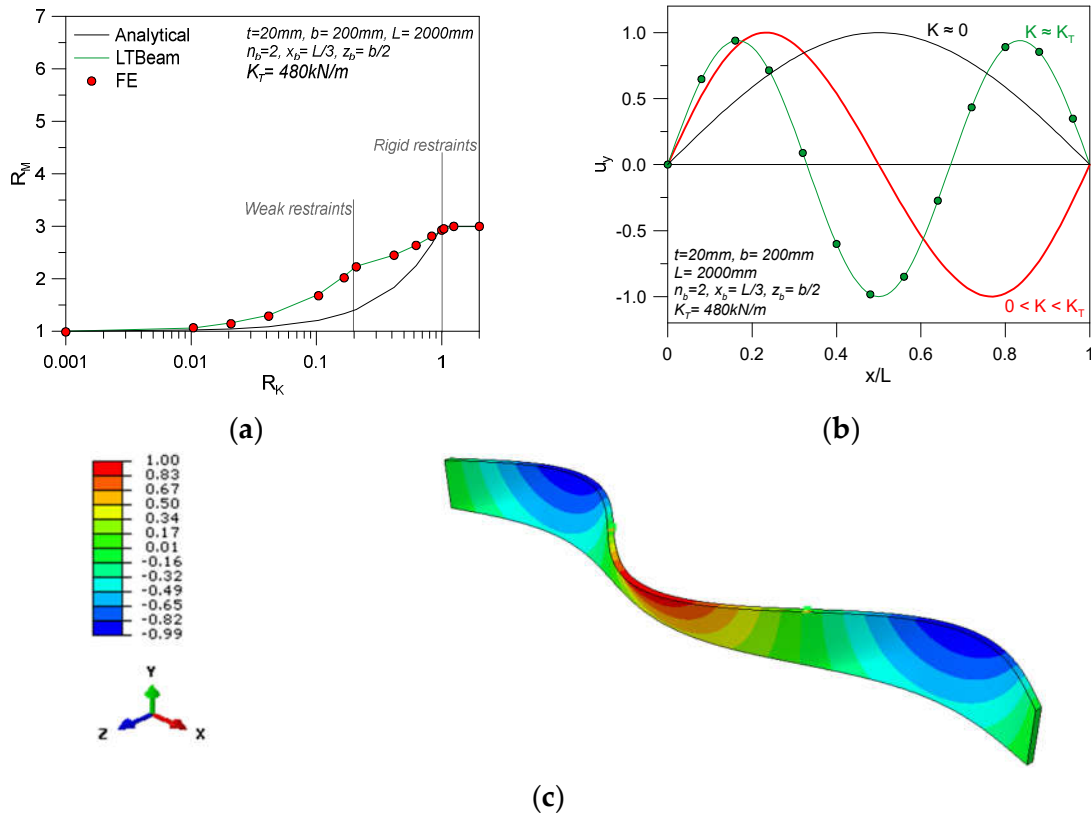


Figure 18. Comparative LTB calculations for LR glass beams with $n_b = 2$ discrete lateral restraints (with $K = \text{var}$): effects on (a) theoretical buckling resistance and critical deformed shapes (from (b) LTBeam or (c) ABAQUS respectively).

At the same time, the FE calculations give evidence of two different variations in the slope of numerical trends. As long as the restraints are weak, compared to the beam configuration, an increase in critical moment is appreciable, but no marked variations are expected for the global LTB response of the member (Figure 18b). Rigid restraints, on the other hand, are associated with a fully rigid bracing system and a typical LTB deformed shape with null local displacements for the n_b restrained nodes (Figure 18c). The intermediate configurations, accordingly, are characterized by a moderate increase of the expected critical buckling moment, as well as by a global LTB deformed shape that presents a partial bracing effect for the regions of LR supports (Figure 18b). Parametric calculations were, thus, repeated for all the previously defined beam geometries, so as to assess the expected scatter due to the approximation induced by the simplified analytical calculations. The so-obtained results are proposed in Figure 19, grouped by beam geometry.

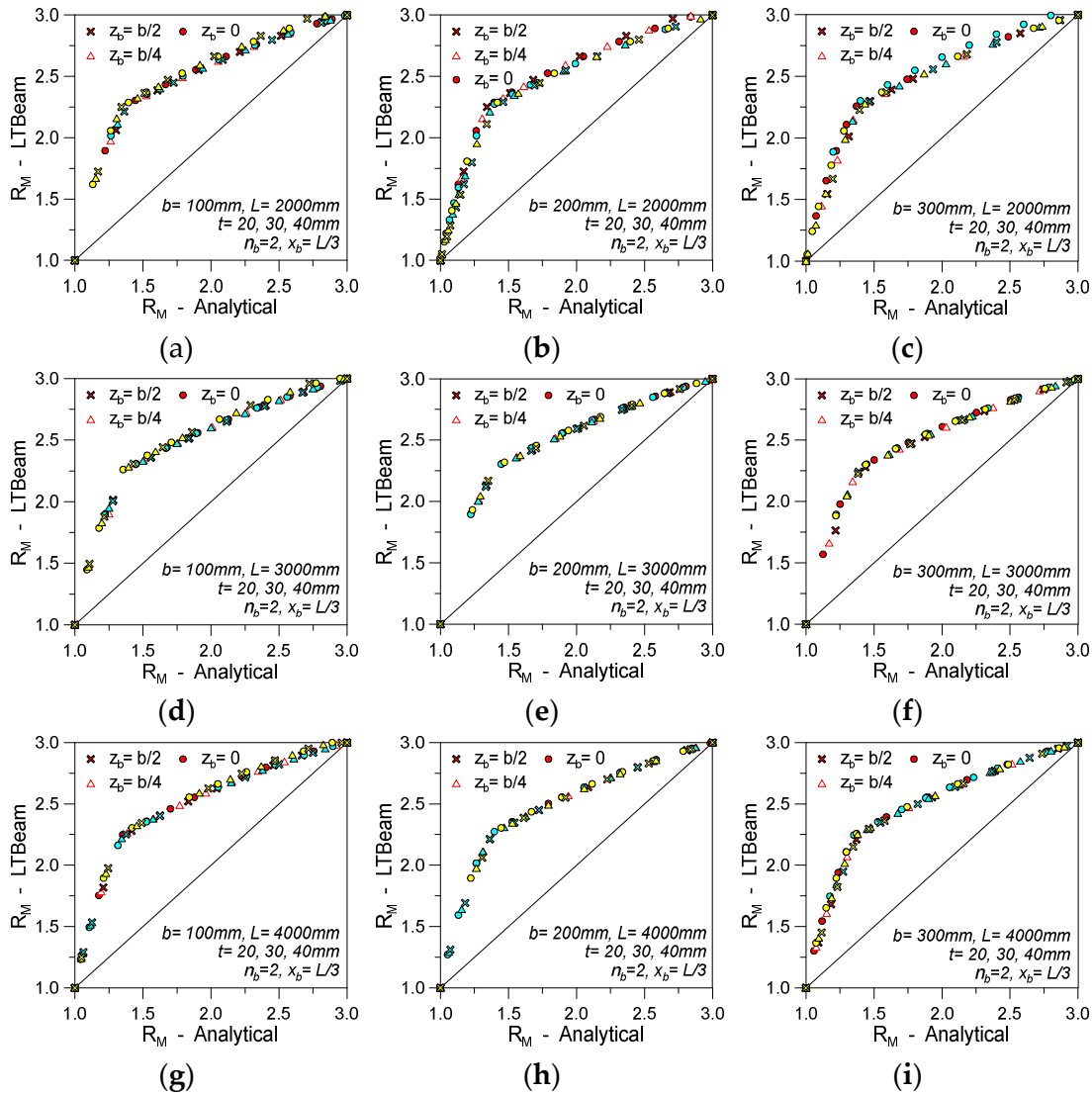


Figure 19. Comparative R_M calculations for LR glass beams in LTB ($n_b = 2, K = \text{var}$).

Differing from Section 5, a relatively high scatter was observed between the so-calculated critical buckling moments, especially in the presence of relatively weak restraints. In Figure 20, the scatter values given by Equation (28) are grouped by span L for the selected beams. As shown, the linearized approach underestimates, by up to 10–15%, the critical moment for R_K values higher than 0.7 (i.e., rigid restraints). The percentage scatter linearly increases (with up to a maximum of 60–70%) in the presence of relatively weak restraints ($R_K = 0.1–0.2$). Worthy of interest, in Figure 20, is the stable trend of the comparative dots, even for discrete restraints having different positions z_b on the beam height. In this regard, the linearized approach could still be used for LTB elastic calculations, as long as the general trend of Figure 20 is taken into account.

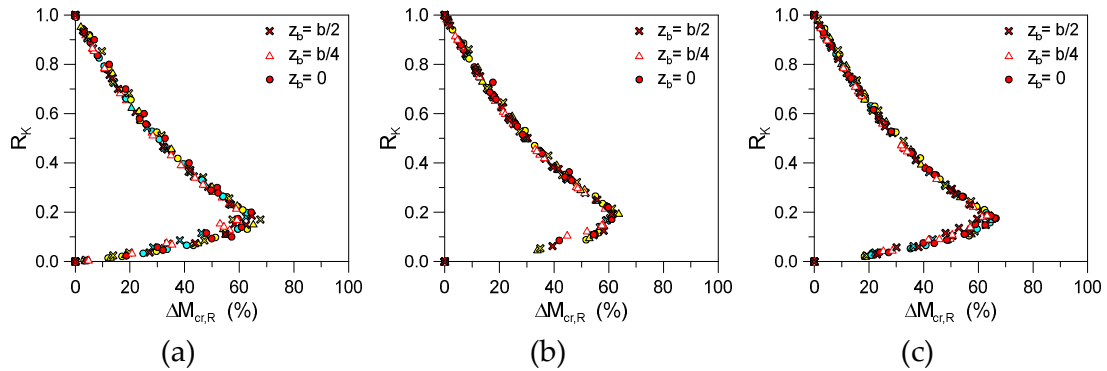


Figure 20. Percentage scatter (Equation (28)) for critical buckling moment estimates of selected LR glass beams ($n_b = 2$, $K = \text{var}$) grouped by span: (a) $L = 2000$ mm, (b) $L = 3000$ mm, and (c) $L = 4000$ mm (with $t = 20, 30, 40$ mm and $b = 100, 200, 300$ mm).

6.2. More Than Two Restraints ($n_b = 3, 4, 5$)

At the final stage of the study, the attention was focused on LR glass beams characterized by a relatively high number of restraints (up to $n_b = 5$, for the selected spans). In accordance with Figure 21, the parametric study gave evidence of relatively rough calculations from the linearized formulation.

Even in the presence of relatively stiff restraints (i.e., $R_K > 0.7$), the percentage scatter due to the analytical model was found on the order of 15%–20%, compared to FE estimates. Such a scatter (see Figure 21) was found to rapidly increase to 80%–90% for the numerical predictions for weak restraints ($R_K \approx 0.4$), before progressively tending to 0 for extremely weak restraints (with negligible effects for LTB purposes). In parallel, the expected fundamental buckling shape was also found to be progressively modified, moving from the LTB response of a simple LU configuration (i.e., Figure 18d) toward a fully restrained deformed shape characterized by $(n_b + 1)$ half-sine waves.

Among the selected configurations, Figure 22 shows that the presence of relatively weak restraints involves a progressively larger percentage scatter underestimation of critical buckling moments, compared to numerical methods. With respect to Figure 17; Figure 20 (where the maximum expected scatter was found in 8% and 70% of cases for glass beams with $n_b = 1$ or $n_b = 2$ weak restraints, respectively), such a percentage value increased to ~90%, ~115%, and ~150% for members characterized by $n_b = 3, 4$, or 5 discrete restraints. In the presence of stiff devices (i.e., $R_K > 0.4$), as shown in Figure 22, the calculated scatter variation is mostly linear with R_K . Accordingly, the comparative results herein summarized could still offer a reliable feedback for simplified but still accurate critical buckling moment estimates on LR glass members in LTB.

6.3. Final Considerations

In conclusion, this research study highlighted some of the major issues that should be accounted for in the LTB analysis of structural glass members with discrete mechanical lateral restraints.

As long as the reliability of simplified analytical or numerical approaches that could be used for the calculation of the theoretical critical buckling resistance or LR glass beams are preliminarily addressed, it is important to further highlight that the same attention should be focused on the non-linear analysis of the same LR braced systems. As known, the knowledge of theoretical buckling loads is in fact a key step for design, but still poor information, compared to the actual load-bearing LTB response and resistance that LR glass members could offer. Major effects are expected, in this sense, from the shape and amplitude of initial geometrical imperfections to account for in non-linear LTB calculations. Moreover, another influencing parameter is expected to derive from the region of holes in glass members, where the stress peaks in LTB should be locally assessed, toward the overall validation of the standardized design approach recalled in Figure 3. Finally, the LTB response of LR glass members subjected to loading and boundary configurations differing from Figure 3 should also be separately investigated.

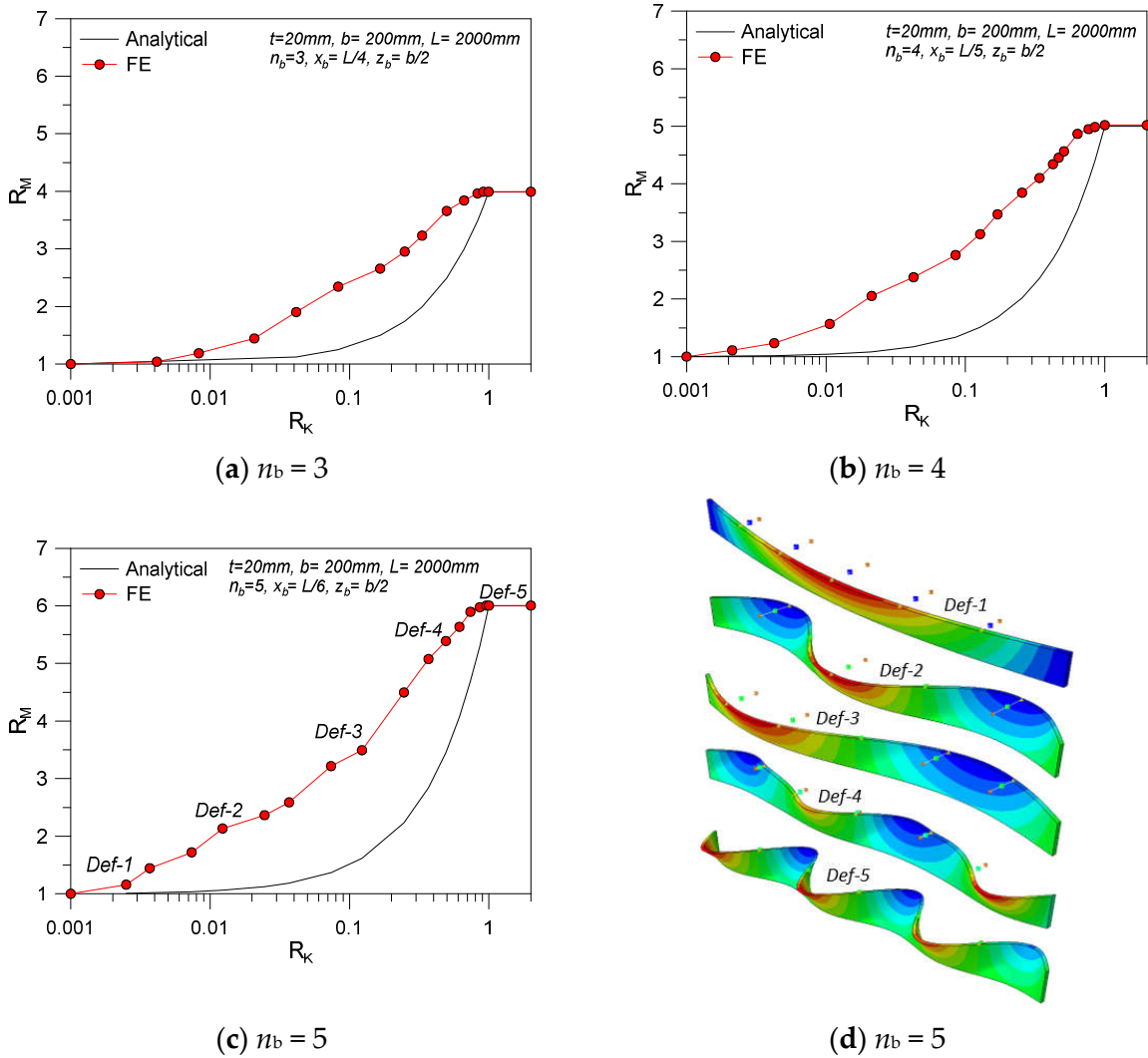


Figure 21. Comparative LTB calculations for LR glass beams with $n_b > 1$ discrete lateral restraints (with $K = \text{var}$): effects on (a–c) theoretical resistance and (d) selected critical deformed shapes (ABAQUS).

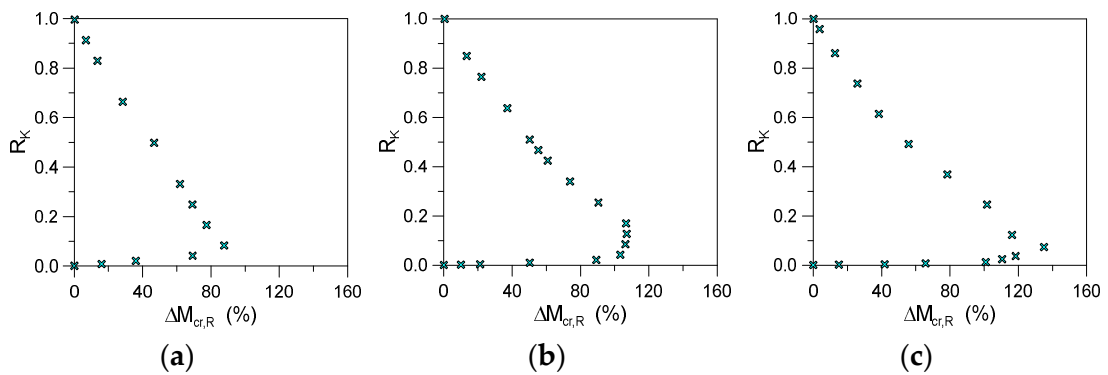


Figure 22. Percentage scatter (Equation (28)) for critical buckling moment estimates of selected LR glass beams ($K = \text{var}$): (a) $n_b = 3$, (b) $n_b = 4$, and (c) $n_b = 5$.

6. Conclusions

The assessment of the lateral–torsional buckling (LTB) behavior of structural glass members represents a key step for design, given the relatively high slenderness of load-bearing members that are typically used in constructions. In addition to such a design issue, most of the literature studies and design recommendations are available in documents and standards for laterally unrestrained (LU) glass members only, thus fully disregarding the effect (and potential) of discrete mechanical restraints that act as lateral bracing systems for laterally restrained (LR) glass members. In addition, an accurate estimation of the theoretical LTB critical moment for such LR systems represents a first key step for design. Often, however, the availability of simplified (but accurate) calculation approaches can offer robust support for designers.

In this paper, the attention was, thus, on the calculation of the elastic critical buckling moment of LR glass beams in LTB. A major advantage was taken from existing analytical approaches of the literature (even mostly developed for steel constructional members), as well as finite element (FE) numerical analyses, which were performed via the LTBeam tool and the ABAQUS computer software.

Based on parametric calculations carried out on a wide series of geometrical and mechanical configurations of technical interest, the actual role and the effect of discrete mechanical restraints were explored for selected LR glass beams. Practical expressions were proposed to assess the expected stiffness contribution of selected mechanical point fixings in use for glass applications. In this regard, the reliability of simplified, spring-based numerical models was validated for selected configurations.

Moreover, the comparative analyses showed that the stiffness, number, and position of discrete mechanical restraints can have marked effects on the expected LTB estimates, with respect to traditional LU glass members. In addition, the use of a linearized analytical formulation (which was further adapted in this paper for LR glass beams) was found to offer rather good predictions, especially for members with single mechanical restraint (with a maximum 7–8% underestimation of theoretical critical moment). In the presence of two discrete restraints, the scatter of analytical estimates was observed to be still reliable for relatively stiff (or very weak, and thus negligible) restraints, while underestimates up to 60% were generally collected for intermediate stiffness configurations. Finally, the analysis of LR glass beams with multiple discrete restraints (up to five) typically resulted in even more pronounced scatter increases, as well as relatively high percentage errors (up 15–20%) for LR glass members with relatively stiff connectors. Furthermore, the trend of the so-calculated scatter was found to be relatively stable for several combinations of geometrical and mechanical parameters of technical interest. As such, the comparative studies herein summarized could represent useful feedback for practical LTB estimates.

Author Contributions: The paper results from a joint collaboration of all the involved authors (D.S., S.M., and C.B.). The research study derives from a past BSc Thesis (D.S.) and an ongoing Ph.D. project (S.M.) carried out at University of Trieste (C.B. supervisor). All authors have read and agreed to the published version of the manuscript.

Funding: This research received no external funding.

Acknowledgments: This paper was submitted, under invitation, for consideration in the MDPI Special Issue call “Modeling and Testing of Laminated Glass”. In this regard, the Guest Editors Prof. Ing. Jan Zeman and Prof. Ing. Michal Šejnoha are gratefully acknowledged for giving this opportunity. MPDI is also acknowledged for the APC discount.

Conflicts of Interest: The authors declare no conflicts of interest.

References

1. Haldimann, M.; Luible, A.; Overend, M. *Structural Use of Glass*; IABSE – International Association for Bridge and Structural Engineering: Zurich, Switzerland, 2008; ISBN 978-3-85748-119-2.
2. CEN/TC 250. *prCEN/TS xxx-1: 2019—In-Plane Loaded Glass Components (December 2019)*; CEN—European Committee for Standardization: Brussels, Belgium, 2019.

3. CEN/TC 250. *prCEN/TS xxxx-2: 2019—Out of-Plane Loaded Glass Components (December 2019)*; CEN—European Committee for Standardization: Brussels, Belgium, 2019.
4. Langosch, K.; Dimova, S.; Pinto Artur, V.; Siebert, G.; Kasper, R.; Louter, C.; Royer-Carfagni, G.; Abeln, B.; Rajcic, V.; Hoegner, H.; et al. *Guidance for European Structural Design of Glass Components—Support to the Implementation, Harmonization and Further Development of the Eurocodes*; Report EUR 26439—Joint Research Centre-Institute for the Protection and Security of the Citizen; Dimova, S., Pinto, A., Feldmann, M., Denton, S., Eds.; European Union: Luxembourg, 2014, doi:10.2788/5523.
5. CNR-DT 210/2013. *Istruzioni per la Progettazione. l'Esecuzione ed il Controllo di Costruzioni con Elementi Strutturali in Vetro [Guideline for Design, Execution and Control of Constructions Made of Structural Glass Elements (in Italian)]*; National Research Council (CNR): Roma, Italy, 2013.
6. Buildings Department. Code of Practice for the Structural Use of Glass. 2018. Available online: <http://www.bd.gov.hk/> (accessed on 25 April 2020).
7. AIS Glass. Code of Practice for Use of Glass in Buildings. 2011. Available online: <https://www.aisglass.com/sites/default/files/pdfs/technical%20papers/AIS-59.pdf> (accessed on 25 April 2020).
8. Martín, M.; Centelles, X.; Solé, A.; Barreneche, C.; Fernández, A.I.; Cabeza, L.F. Polymeric interlayer materials for laminated glass: A review. *Constr. Build. Mater.* **2020**, *230*, 116897, doi:10.1016/j.conbuildmat.2019.116897.
9. Kuntsche, J.; Schuster, M.; Schneider, J. Engineering design of laminated safety glass considering the shear coupling: A review. *Glass Struct. Eng.* **2019**, *4*, 298–228.
10. Hänig, J.; Bukieda, P.; Engelmann, M.; Stelzer, I.; Weller, B. Examination of Laminated Glass with Stiff Interlayers – Numerical and Experimental Research. *Int. J. Struct. Glass Adv. Mater. Res.* **2019**, *3*, 1–14, doi:10.3844/sgamrsp.2019.1.14.
11. Hána, T.; Eliášová, M.; Sokol, Z. Structural Performance of Double Laminated Glass Panels with EVA and PVB Interlayer in Four-Point Bending Tests. *Int. J. Struct. Glass Adv. Mater. Res.* **2018**, *2*, 164–177, doi:10.3844/sgamrsp.2018.164.177.
12. Hána, T.; Janda, T.; Schmidt, J.; Zemanová, A.; Šejnoha, M.; Eliášová, M.; Vokáč, M. Experimental and Numerical Study of Viscoelastic Properties of Polymeric Interlayers Used for Laminated Glass: Determination of Material Parameters. *Materials* **2019**, *12*, 2241, doi:10.3390/ma12142241.
13. Dural, E. Analysis of delaminated glass beams subjected to different boundary conditions. *Compos. Part B Eng.* **2016**, *101*, 132–146.
14. Bedon, C. Issues on the Vibration Analysis of In-Service Laminated Glass Structures: Analytical, Experimental and Numerical Investigations on Delaminated Beams. *Appl. Sci.* **2019**, *9*, 3928, doi:10.3390/app9183928.
15. Sable, L.; Kinsella, D.; Kozłowski, M. Influence of EVA, PVB and Ionoplast Interlayers on the Structural Behaviour and Fracture Pattern of Laminated Glass. *Int. J. Struct. Glass Adv. Mater. Res.* **2019**, *3*, 62–78, doi:10.3844/sgamrsp.2019.62.78.
16. Belis, J. *Kipsterkte van Monolithische en Gelamineerde Glazen Liggers*; Ghent University: Ghent, Belgium, 2005.
17. Belis, J.; Bedon, C.; Louter, C.; Amadio, C.; van Impe, R. Experimental and analytical assessment of lateral torsional buckling of laminated glass beams. *Eng. Struct.* **2013**, *51*, 295–305.
18. Pešek, O.; Melcher, J. Lateral-torsional buckling of laminated structural glass beams. Experimental study. *Procedia Eng.* **2017**, *190*, 70–77.
19. Rosati, G.; Orlando, M.; Piscitelli, L.R. Flexural-torsional buckling tests on laminated glass beams. Glass on Web. 2013. Available online: <https://www.glassonweb.com/article/flexural-torsional-buckling-tests-laminated-glass-beams> (accessed on 25 April 2020).
20. Horcicková, I.; Eliášová, M. Lateral and torsional stability of glass beams. In Proceedings of the 53rd Conference on Experimental Stress Analysis, Český Krumlov, Czech Republic, 1–4 June 2015, pp. 130–133.
21. Valarihno, L.; Correia, J.R.; Machado-e-Costa, M.; Branco, F.A.; Silvestre, N. Lateral-torsional buckling behaviour of long-span laminated glass beams: Analytical, experimental and numerical study. *Mater. Des.* **2016**, *102*, 264–275.
22. Bedon, C.; Belis, J.; Luible, A. Assessment of existing analytical models for the lateral torsional buckling analysis of PVB and SG laminated glass beams via viscoelastic simulations and experiments. *Eng. Struct.* **2014**, *60*, 52–67.

23. Amadio, C.; Bedon, C. Buckling of laminated glass elements in out-of-plane bending. *Eng. Struct.* **2010**, *32*, 3780–3788.
24. Luible, A.; Crisinel, M. *Design of Glass Beams Subjected to Lateral Torsional Buckling*; IABSE Symposium “Responding to Tomorrow’s Challenges in Structural Engineering”, Report n. 92; Budapest, Hungary, 2006; pp. 45–53. IABSE– International Association for Bridge and Structural Engineering; Zurich, Switzerland
25. Bedon, C.; Amadio, C. Design buckling curves for glass columns and beams. *Struct. Build.* **2015**, *168*, 514–526.
26. Riddell-Smith, L.; Cunningham, L.S.; Mandal, P. Design of glass elements for lateral-torsional buckling: Review of existing approaches. *J. Archit. Eng.* **2017**, *23*, doi:10.1061/(ASCE)AE.1943-5568.0000255.
27. Bedon, C.; Belis, J.; Amadio, C. Structural assessment and lateral-torsional buckling design of glass beams restrained by continuous sealant joints. *Eng. Struct.* **2015**, *120*, 214–229.
28. Bedon, C.; Amadio, C. Analytical and numerical assessment of the strengthening effect of structural sealant joints for the prediction of the LTB critical moment in laterally restrained glass beams. *Mater. Struct.* **2015**, 10.1617/s11527-015-0661-z.
29. Sonck, D.; Belis, J. Elastic lateral-torsional buckling of glass beams with continuous lateral restraints. *Glass Struct. Eng.* **2016**, *1*, 173–194.
30. Luible, A.; Schärer, D. Lateral torsional buckling of glass beams with continuous lateral support. *Glass Struct. Eng.* **2016**, *1*, 153–171.
31. Belis, J.; van Impe, R.; Lagae, G.; Vanlaere, W. Enhancement of the buckling strength of glass beams by means of lateral restraints. *Struct. Eng. Mech.* **2003**, *15*, 495–511.
32. McCann, F. Stability of Beams with Discrete Lateral Restraints. Ph.D. Thesis, Imperial College London, London, UK, 2012.
33. McCann, F.; Gardner, L.; Wade, M.A. Design of steel beams with discrete lateral restraints. *J. Constr. Steel Res.* **2013**, *80*, 82–90.
34. LTBeam Freeware Software. Available online: <https://www.cticm.com/logiciel/ltbeam/> (accessed on 25 April 2020).
35. Simulia. *Dassault Systemes*; Providence, RI, USA, 2020.
36. EN 1993-1-1: 2005. *Eurocode 3 – Design of Steel Structures – Part 1–1: General Rules and Rules for Buildings*; May 2005; CEN – European Committee for Standardization; Brussels, Belgium, 2005.
37. Galuppi, L.; Manara, G.; Royer, G. Practical expressions for the design of laminated glass. *Compos. Part B Eng.* **2013**, *45*, 1677–1688.
38. Luible, A. *Stabilität von Tragelementen aus Glas*; Ecole Polytechnique Fédérale de Lausanne: Lausanne, Switzerland, 2004.
39. Bedon, C.; Amadio, C. Flexural–torsional buckling: Experimental analysis of laminated glass elements. *Eng. Struct.* **2014**, *73*, 85–99.
40. Valentino, J.; Pi, Y.L.; Trahair, N.S. Inelastic buckling of steel beams with central torsional restraints. *J. Struct. Eng.* **1997**, *123*, doi:10.1061/(ASCE)0733-9445(1997)123:9(1180).
41. Lindner, J. *Lateral Torsional Buckling of Steel Beams and Rectangular Glass Beams Consisting of Single Panes - A Comparison*. *Steel - A New and Traditional Material for Building*; Dan Dubina & Viorel Ungureanu Eds.; 2006; pp. 199–205, ISBN 0-415-40817-2. Taylor & Francis Group, London, UK
42. Bruins, R.H.J. Lateral-Torsional Buckling of Laterally Restrained Steel Beams. Master’s Thesis, Eindhoven University of Technology, Eindhoven, The Netherlands, 2005.
43. Trahair, N.S. *Flexural-Torsional Buckling of Structures*; E & FN SPON: London, UK, 1993.
44. Handbook, P. Teflon PTFE. Available online: http://www.rjchase.com/ptfe_handbook.pdf. (accessed on 25 May 2020).
45. Rae, P.J.; Dattelbaum, D.M. The properties of poly (tetrafluoroethylene) (PTFE) in compression. *Polymer* **2004**, *45*, 7615–7625.
46. Hernández-Jiménez, A.; Hernández-Santiago, J.; Macías-García, A.; Sánchez-González, J. Relaxation modulus in PMMA and PTFE fitting by fractional Maxwell model. *Polym. Test* **2002**, *21*, 325–331.
47. Nunes, L.C.S.; Dias, F.W.R.; da Costa Mattos, H.S. Mechanical behavior of polytetrafluoroethylene in tensile loading under different strain rates. *Polym. Test.* **2011**, *30*, 791–796.
48. Ge, C.; Maimaitituersun, W.; Dong, Y.; Tian, C. A Study on the Mechanical Properties and Impact-Induced Initiation Characteristics of Brittle PTFE/Al/W Reactive Materials. *Materials* **2017**, *10*, 452, doi:10.3390/ma10050452.

49. Krempl, E.; Khan, F. Rate (time)-dependent deformation behavior: An overview of some properties of metals and solid polymers. *Int. J. Plast.* **2003**, *19*, 1069–1095.
50. EN 572-2:2004. *Glass in Buildings – Basic Soda Lime Silicate Glass Products*; CEN – European Committee for Standardization: Brussels, Belgium, 2004.
51. EN 10088-2: 2014. *Stainless Steels - Part 2: Technical Delivery Conditions for Sheet/Plate and Strip of Corrosion Resisting Steels for General Purposes*; CEN – European Committee for Standardization: Brussels, Belgium, 2014.



© 2020 by the authors. Licensee MDPI, Basel, Switzerland. This article is an open access article distributed under the terms and conditions of the Creative Commons Attribution (CC BY) license (<http://creativecommons.org/licenses/by/4.0/>).